



RESEARCH & DEVELOPMENT

Improved Approaches to Environmental Compliance During Highway Construction

**Richard A. McLaughlin
Department of Crop and Soil Sciences**

**North Carolina State University
Raleigh, North Carolina**

**NCDOT Project 2019-05
FHWA/NC/2019-05
April 2021**

**IMPROVED APPROACHES TO ENVIRONMENTAL
COMPLIANCE DURING HIGHWAY CONSTRUCTION**

North Carolina Department of Transportation

Project Authorization No. HWY-2019-05

Principal Investigator

Richard A. McLaughlin, Ph.D.

Department of Crop and Soil Sciences

North Carolina State University

Raleigh, North Carolina

Technical Report Documentation Page

1. Report No. FHWA/NC/2019-05	2. Government Accession No.	3. Recipient's Catalog No.
4. Title and Subtitle Improved Approaches to Environmental Compliance During Highway Construction		5. Report Date April 8, 2021
7. Author(s) Richard A. McLaughlin, Jalen Hairston, Chris Niewoehner, and Greg Lucier		6. Performing Organization Code
9. Performing Organization Name and Address Crop and Soil Sciences Dept., Box 7620, North Carolina State University Raleigh, NC 27695		8. Performing Organization Report No.
12. Sponsoring Agency Name and Address North Carolina Department of Transportation Research and Development Unit 104 Fayetteville Street Raleigh, North Carolina 27601		10. Work Unit No. (TRAIS)
Supplementary Notes:		11. Contract or Grant No.
		13. Type of Report and Period Covered Final Report August 2018 – March 2021
		14. Sponsoring Agency Code 2019-05

16. Abstract

This project encompassed investigations into a variety of practices currently in use or with potential applications to managing construction site stormwater. Dust control is necessary during dry periods on construction site haul roads, and is currently controlled by constant applications of water by tanker trucks. Three dust control products with different properties were tested using simple application methods. CaCl_2 was the one product that consistently reduced dust by 30-50% for periods of several weeks after application. Any effect of water disappeared too quickly to be detected. Site inspections are labor intensive, so we investigated the potential for using an unmanned aerial vehicle (UAV) for inspecting erosion and sediment control devices. The UAV generally reduced the total time for inspections and detected similar numbers of issues as on-foot inspections, with the exception of silt fence tears and holes. A hybrid approach may be the optimal use of this technology. The UAV data was also used to estimate watershed size for sediment basins and silt fence outlets as a site was graded. The changing landscape resulted in under- or over-sized watersheds for device design over time. This was further explored for five sediment basins by monitoring their volume change during storm events which did not overtop the auxiliary spillway (weir). For these events, usually $<1''$ of rain, less than 50% of the rain volume reached the basin. As expected, higher intensity storms generated a higher runoff volume. Fence posts which are or could be used for silt fences were tested to determine how much force they could withstand relative to the amount expected with a full 2' of water behind the fence. The current standard (1.25 lb ft^{-1}) steel post can handle that amount of ponding on 8' spacing, as well as a heavier steel post. A lighter (0.86 lb ft^{-1}) steel post failed at just under the maximum force (2' of water, 8' spacing) but was sufficient at closer spacing. A 1.5x1.5" wood post can withstand this force up to a 6' spacing, but the 1x1" wood post was insufficient at any spacing. The pressure on the silt fence drops exponentially with water depth, so at a 1.5' pool depth, even the smaller wood post had sufficient strength.

17. Key Words

Wildflowers, pollinators, tillage, infiltration

18. Distribution Statement

19. Security Classif. (of this report)
Unclassified

20. Security Classif. (of this page)
Unclassified

21. No. of Pages
81

22. Price

Disclaimer

The contents of this report reflect the views of the author(s) and not necessarily the views of the University. The author(s) are responsible for the facts and the accuracy of the data presented herein. The contents do not necessarily reflect the official views or policies of either the North Carolina Department of Transportation or the Federal Highway Administration at the time of publication. This report does not constitute a standard, specification, or regulation.

Acknowledgements

This project involved a large number of people in order to achieve our objectives. Key staff were Jamie Luther and Chris Niewoehner, who kept the field and lab work moving forward at all stages. Graduate student Jalen Hairston with assistance from Research Associate Rob Austin were instrumental in performing the UAV evaluations. Research Associate Professor Greg Lucier and staff performed all of the fence post testing and wrote up that part of this report. For the roadside studies, NCDOT staff were very helpful in locating suitable sites. Recognition of the need for research and funding to support it has been and continues to be a reason NCDOT is among the leaders in environmental and water quality improvements associated with our transportation systems.

Executive Summary

This project encompassed investigations into a variety of practices currently in use or with potential applications to managing construction site stormwater. Dust control is necessary during dry periods on construction site haul roads, and is currently controlled by constant applications of water by tanker trucks. Three dust control products with different properties were tested using simple application methods. CaCl_2 was the one product that consistently reduced dust by 30-50% for periods of several weeks after application. Any effect of water disappeared too quickly to be detected. Site inspections are labor intensive, so we investigated the potential for using an unmanned aerial vehicle (UAV) for inspecting erosion and sediment control devices. The UAV generally reduced the total time for inspections and detected similar numbers of issues as on-foot inspections, with the exception of silt fence tears and holes. A hybrid approach may be the optimal use of this technology. The UAV data was also used to estimate watershed size for sediment basins and silt fence outlets as a site was graded. The changing landscape resulted in under- or over-sized watersheds for device design over time. This was further explored for five sediment basins by monitoring their volume change during storm events which did not overtop the auxiliary spillway (weir). For these events, usually $<1''$ of rain, less than 50% of the rain volume reached the basin. As expected, higher intensity storms generated a higher runoff volume. Fence posts which are or could be used for silt fences were tested to determine how much force they could withstand relative to the amount expected with a full 2' of water behind the fence. The current standard (1.25 lb ft^{-1}) steel post can handle that amount of ponding on 8' spacing, as well as a heavier steel post. A lighter (0.86 lb ft^{-1}) steel post failed at just under the maximum force (2' of water, 8' spacing) but was sufficient at closer spacing. A $1.5 \times 1.5''$ wood post can withstand this force up to a 6' spacing, but the $1 \times 1''$ wood post was insufficient at any spacing. The pressure on the silt fence drops exponentially with water depth, so at a 1.5' pool depth, even the smaller wood post had sufficient strength.

Conclusions

The following are the recommendations based on our studies:

1. Dust control products based on moisture retention show promise for applications on haul roads. The tests conducted in this project only involved surface applied granular CaCl_2 , and some agencies suggest incorporating it into the surface for best results.
2. Aerial photography from UAVs for weekly site erosion and sediment control inspections has a number of advantages over on-foot inspections, including a record of the devices, flying when the site is too muddy for vehicles, and detection of some issues more easily. Compromised silt fences (holes, tears) were less obvious by UAV, but adjusting camera angles might reduce this problem. Using structure through motion software, watershed area for devices can be calculated and diversions installed if they area exceeds device design.
3. Sediment basins received surprisingly low proportions of rainfall volume, less than 50%, for events that did not overtop the auxiliary spillway in skimmer basins. All five of the tested basins had watersheds with some portion stabilized by mulch or vegetation, suggesting this practice is effective. Runoff volumes for events that did overtop the

spillway were not measured, but clearly higher proportions of rainfall reached the basins during high intensity 1-2" hr⁻¹ periods.

4. The current standard for silt fence posts, 1.25 lb ft⁻¹, exceeds the performance needed to restrain 2' of pooled water and 8' post spacings. Lighter steel posts and wood posts could be used for closer spacings or if release devices prevent pooling to the full 2'.

Table of Contents

Title Page	2
Technical Report Documentation Page	3
Disclaimer	5
Acknowledgements	6
Executive Summary	7
Chapter 1: Testing Dust Control Products	16
Chapter 2: UAV Applications on Construction Sites	26
Chapter 3: Sediment Basin Hydrology	53
Chapter 4: Fence Post Testing	69

Table of Figures

Figure 1.0. Examples of dump trucks generating dust on a haul road.....	16
Figure 1.1 Aerial view of the Chi Road test site showing the two blocks.....	17
Figure 1.2 Location of each treatment within each block for the first test on Chi Road.....	17
Figure 1.3 Location of each treatment within each block for the second test on Chi Road.....	18
Figure 1.4 Aerial view of the Mid Pines Road test site and location of blocks.....	18
Figure 1.5 Location of each treatment within each block for the test on Mid Pines Road.....	19
Figure 1.6 Cutaway view of the dust collectors used in this study.....	20
Figure 1.7 Dust collection at the Chi Road site.....	21
Figure 1.8 Dust reduction for treatments on Chi Road as a fraction of the untreated control during the first test period.....	24
Figure 1.9 Dust reductions for treatments on Chi Road as a fraction of the untreated control during the second test period.....	24
Figure 1.10 Dust reduction for treatments on Mid-Pines Road as a fraction of the untreated control section.....	25
Figure 2.0 The effect of using ground control points to correct vertical accuracy for the MPP and PRTK UAVs at 60 m and 120m.....	39
Figure 2.1 The effect of overlap and ground control points on horizontal accuracy for the MPP and PRTK UAVs at 60 m and 120 m.....	40
Figure 2.2 Example of a wattle failure with undercutting and ditch erosion at the NC 42 site.....	43
Figure 2.3 Example of baffle failure due to placement of a slope drain on top of the baffle.....	44
Figure 2.4 Example of heavy sediment deposition on one side of a Type C Rock Inlet Protection device.....	44
Figure 2.5 Elevation changes at the borrow pit from March 23 to June 12, 2020.....	46
Figure 2.6 US 401 borrow pit area showing locations of various sediment basins and silt fence outlets (SF). The ground control and check points were used to determine the accuracy of locations by the MPP (discussed earlier).....	48
Figure 2.7 Watershed delineation of basins and sediment fence outlets as of 03.16.20 for US-401 borrow pit.....	50
Figure 2.8 Photo of the breach in the diversion for Basin 1D.....	51
Figure 3.0. Regression of basin water level with volume in the basin.....	54

Figure 3.1. Picture of Basin 1 after a runoff event. Heavy winds were creating a choppy surface.....	55
Figure 3.2. Picture of Basin 2 between runoff events.....	55
Figure 3.3. Picture of Basin 3 at one of the two inlets. Sampler tubing can be seen along the top of the first baffle.....	56
Figure 3.4. Picture of Basin 4 showing the samplers and rain gauges.....	56
Figure 3.5. Picture of Borrow Pit Basin during skimmer discharge period.....	57
Figure 3.6. Watershed for Basin 2, showing the two different drainage areas.....	58
Figure 3.7. Basin water level and rainfall data for Basins 1 and 2 during the monitoring period.....	60
Figure 3.8. Volume of rainfall in Basin 1 watershed and increase in basin volume for the April 20, 2020 storm. Basin volume increase was approximately 44% of rainfall volume.....	61
Figure 3.9. Volume of rainfall in Basin 1 watershed and increase in basin volume for the July 13, 2020 storm. Basin volume increase was approximately 25% of rainfall volume.....	61
Figure 3.10. Volume of rainfall in Basin 2 watershed and increase in basin volume for the April 20, 2020 storm. Basin volume increase was approximately 26% of rainfall volume.....	62
Figure 3.11. Volume of rainfall in Basin 2 watershed and increase in basin volume for the July 13-14, 2020 storm. Basin volume increase was approximately 12% of rainfall volume.....	62
Figure 3.12. Basin water level and rainfall during the monitoring period at the borrow pit on US 401.....	63
Figure 3.13. Volume of rainfall in the Borrow Pit basin and increase in basin volume for the March 23-25 rainfall event. The drainage area was approximately 8.4 acres for this event. Basin volume increase was approximately 23% of rainfall volume.....	63
Figure 3.14. Volume of rainfall in the Borrow Pit basin and increase in basin volume for the May 18-21 rainfall event. The drainage area was approximately 9.9 acres for this event. Basin volume increase was approximately 17% of rainfall volume.....	64
Figure 3.15. Volume of rainfall in the Borrow Pit basin and increase in basin volume for the September 17-18 rainfall event. Basin volume increase was approximately 20% of rainfall volume.....	64
Figure 3.16. Rainfall and basin water levels for the monitoring period of Basins 3 and 4.....	65
Figure 3.17. Volume of rainfall in Basin 3 and increase in basin volume for the February 12, 2020 rainfall event. Basin volume increase was approximately 45% of rainfall volume.....	66

Figure 3.18. Volume of rainfall in Basin 3 and increase in basin volume for the February 18-20, 2020 rainfall event. Basin volume increase was approximately 37% of rainfall volume.....	66
Figure 3.19. Volume of rainfall in Basin 4 and increase in basin volume for the February 11-12, 2020 rainfall event. Basin volume increase was approximately 50% of rainfall volume.....	67
Figure 3.20. Volume of rainfall in Basin 4 and increase in basin volume for the February 18-20, 2020 rainfall event. Basin volume increase was approximately 34% of rainfall volume.....	67
Figure 3.21. Rainfall rate, basin water level, and estimated runoff rate for Basin 4 during a 2-day rain event totaling 6.17 inches of rain. Discharge over the weir occurred slightly lower than three feet.....	68
Figure 4.0: Simplified Fence Post Loading Model, Profile View.....	72
Figure 4.1: Simplified Fence Post Loading Model, Elevation View.....	73
Figure 4.2: Test setup for fence post loading.....	79

List of Tables

Table 1.0	Sampling dates at each location.....	21
Table 1.1	Dust control products used in the study, with application rate and method.....	22
Table 1.2	Rainfall during or between the dust monitoring periods.....	22
Table 2.0.	Camera and technical specifications on how Mavic Pro Platinum operate.....	32
Table 2.1.	Camera and technical specifications of how Phantom 4 RTK operate.....	32
Table 2.2	Flight mission settings that were conducted on NC 42 East’s section 1.....	34
Table 2.3	Comparison of problem detections by either UAV or on-foot inspections of nine common BMPs on the NC 42 site.....	41
Table 2.4	Comparison of problem detections by either UAV or on-foot inspections of nine common BMPs on the US 401 site.....	42
Table 2.5	Comparison of time required to conduct inspections at the NC 42 site. Negative values indicate on-foot was faster, positive that UAV was faster.....	43
Table 2.6	Comparison of time required to conduct inspections at the US 401 site. Negative values indicate on-foot was faster, positive that UAV was faster.....	43
Table 2.7	Volume changes at the borrow pit at US 401 over different time intervals, as estimated by DEMs developed from UAV images or by counting trucks (NCDOT).....	47
Table 2.8	Dimensions and estimated drainage areas at different survey dates for five sediment basins at the borrow pit site. Design drainage area is shown in parentheses below each basin designation.....	49
Table 2.9	Dimensions and estimated drainage areas at different survey dates for seven sediment fence locations at the borrow pit site. Design drainage area is shown in parentheses below each silt fence designation.....	49
Table 3.0.	Example of area calculations for the basins based on depth and resulting area.....	54
Table 3.1.	Watershed areas for the monitored basins based on GIS modeling.....	57
Table 4.0:	GADOT Silt Fence Post Requirements (Specification Section 894).....	70
Table 4.1:	Total Force on a Single Post by Water Height and Post Spacing.....	74

Table 4.2: Maximum Moment Demand for a Single Silt Fence Post.....	75
Table 4.3: Styles of Silt Fence Post Tested.....	76
Table 4.4: Photographs of Typical Tested Silt Fence Posts.....	77
Table 4.5: Properties of Tested Silt Fence Posts.....	77
Table 4.6: Results from Each Silt Fence Post Test.....	79
Table 4.7: Typical Failure Modes for Each Type of Tested Silt Fence Post.....	81
Table 4.8: Load-Deflection Data for All Tested Posts.....	82
Table 4.9: Styles of Silt Fence Post Tested.....	83

List of Equations

Equation 2.0 (Length (m) × Width (m) × Height (m)) ÷ 51m³ =

Drainage Acreage for respective basin.....38

Equation 2.1 (Sediment Fence Length (m) ÷ 30m) × .25ac =

Drainage Acreage for respective sediment fence.....38

Equation 4.0 P = ρH.....72

Equation 4.1 F = ½ P(WxS).....73

Equation 4.2 M = F(1/3xW).....74

Chapter 1. Testing Dust Control Products

Road building often requires considerable amounts of soil being moved around the project to obtain the desired road grade. During dry periods, the dump trucks moving this material can generate large amounts of dust from the haul road (Figure 1.1). The standard practice is to apply water to the road, but this may only control dust emissions for short periods and can create traction issues. There are many dust control products on the market which could provide longer and better dust control, and some evaluations have been conducted on maintained gravel roads (Johnson and Olson, 2009; Sanders et al., 1997).

There are more than 150 products available as unpaved road additives (Jones et al., 2013), some of which could be more effective, more economical, and more environmentally friendly than running water trucks up and down the road. These are widely used in arid areas and the technology may be transferred readily to construction projects in North Carolina. This project involved testing several types of products for dust control. Calcium chloride, as well as magnesium chloride, is used to attract moisture from the atmosphere to the road to keep it sufficiently moist to reduce dust. Polyvinyl acetate represents the types of products which bind to or “glue” the road materials to hold them together to prevent dust generation. Polyacrylamide has been demonstrated to reduce erosion by binding small soil particles together, but it was unclear if this would translate to dust control as well.



Figure 1.0. Examples of dump trucks generating dust on a haul road.

Materials and Methods

The products were tested on two gravel roads at the Lake Wheeler Road Field Laboratory in Raleigh, NC. Two tests were conducted on Chi Road (Fig. 1.1) and another on Mid Pines Road (Fig. 1.3). The general concept at both sites was to generate dust either from a standardized amount of vehicle traffic, the ambient traffic, or a combination. The standardized traffic consisted of a Ford F-150 pickup traveling at 25-35 miles per hour past the samplers for 20

passes. Ambient traffic included everything from small cars to tractor-trailer trucks as well as farm vehicle.

Plots were established on each road for product application. On Chi Road, the plots were 20 feet wide and 100 feet long, with 80 feet between them (Fig. 1.2). On Mid Pines Road, the plots were 22 feet wide and 200 feet long, with no buffer between them (Fig. 1.4). Treatments were applied in a complete randomized block design with two blocks, each including three treatments and an untreated control.

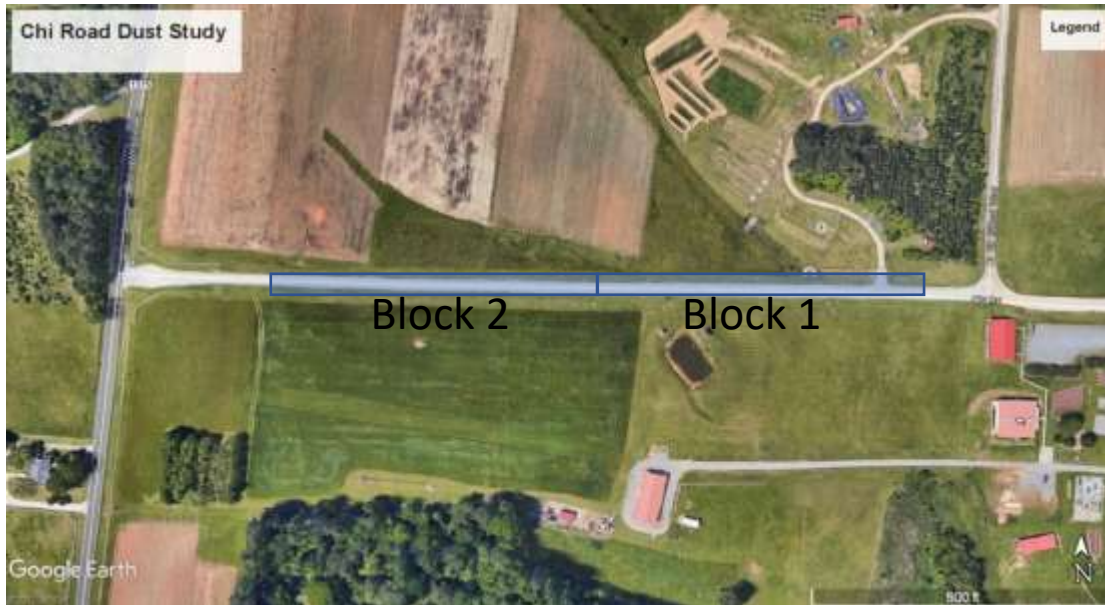


Figure 2.1 Aerial view of the Chi Road test site showing the two blocks.

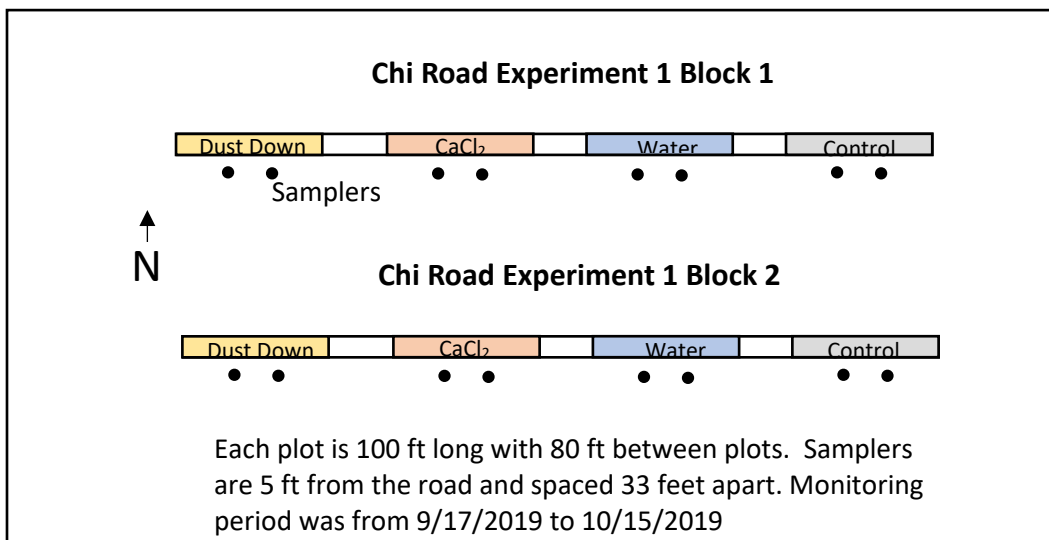


Figure 1.2 Location of each treatment within each block for the first test on Chi Road.

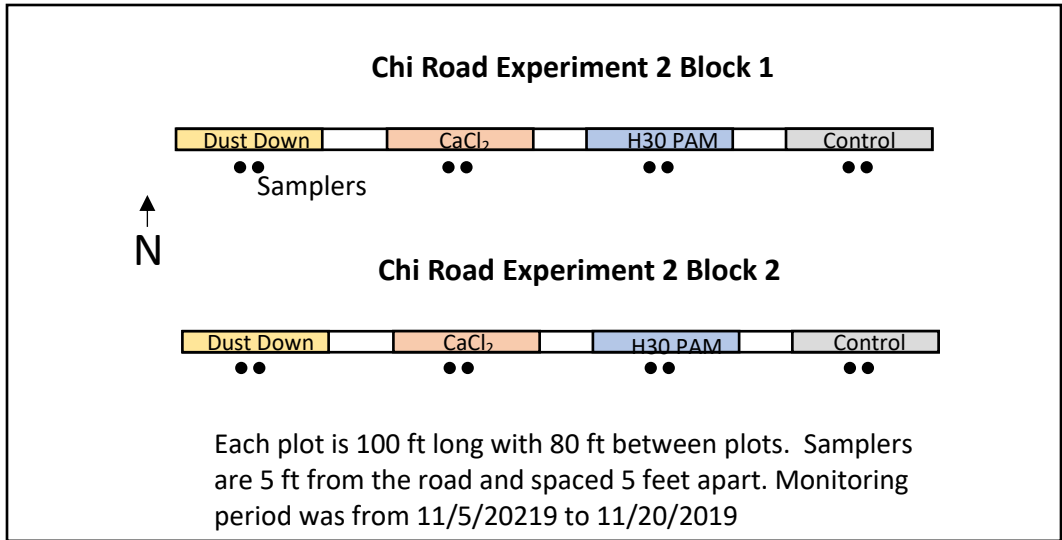


Figure 1.3 Location of each treatment within each block for the second test on Chi Road.

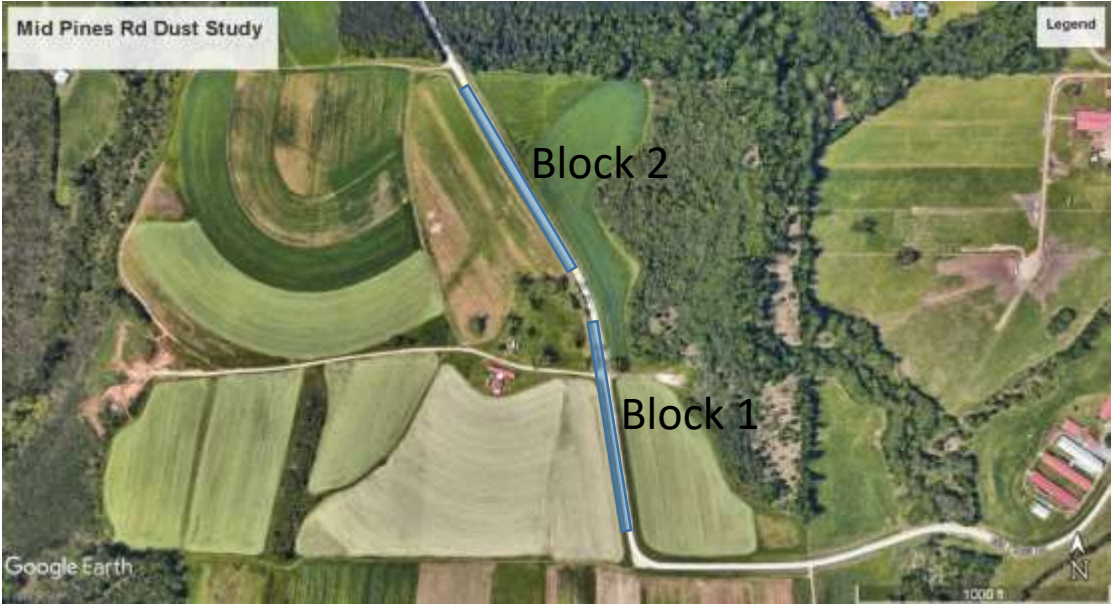


Figure 1.4 Aerial view of the Mid Pines Road test site and location of blocks.

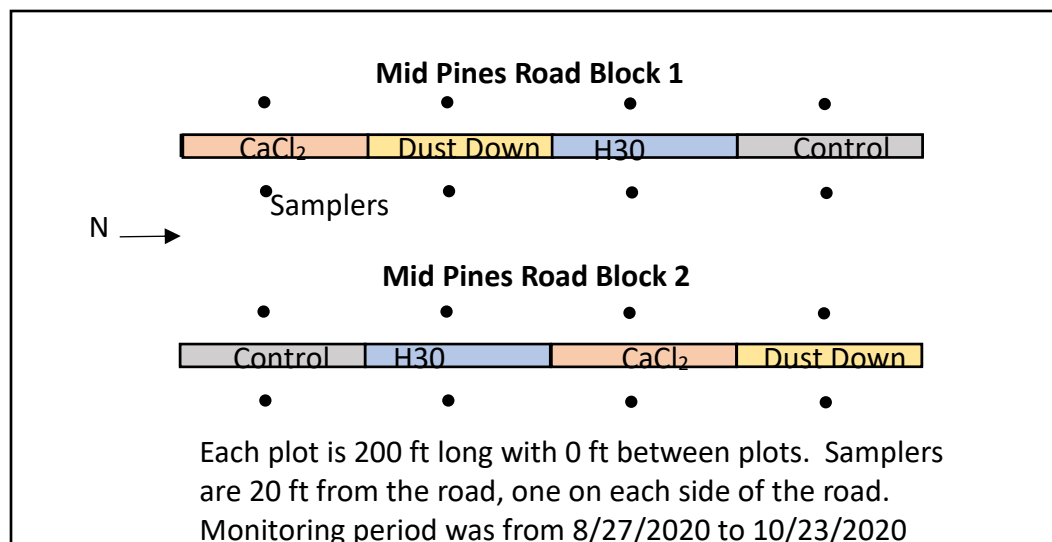
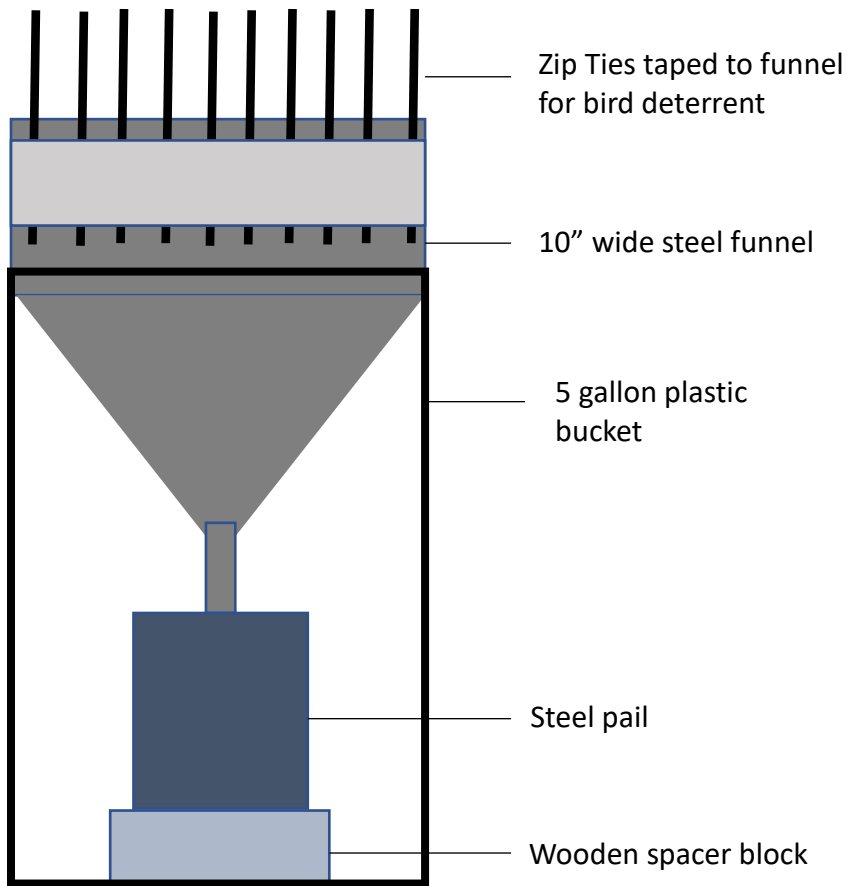


Figure 1.5 Location of each treatment within each block for the test on Mid Pines Road.

Dust was collected using a funnel and bucket system similar to Cruizer et al. (2016). A large metal funnel was placed in a five gallon plastic bucket with a two gallon bucket at the bottom (Figure 1.6). At Chi Road, the entire collector was suspended on a T-post approximately three feet from the ground, adjacent to the road on the south side. At Mid Pines Road, the collectors were attached to existing fence posts on both sides of the road. To collect a dust sample, the funnel and the two gallon dust collector bucket were removed, and the residual dust in the funnel rinsed into the dust collector bucket (Fig 1.7). The rinsate was poured into a sample bottle and taken to the laboratory for analysis. In the lab, the rinsate was filtered through a 1.5 μm glass fiber filter which was dried at 105°C for at least 24 h and then weighed.



Samplers were attached to 5' steel T-Posts with bungee cords for Chi Rd studies, and existing wooden fence posts on Mid Pines Rd

Figure 1.6 Cutaway view of the dust collectors used in this study.



Figure 1.7 Dust collection at the Chi Road site. The funnel was removed (left) and the dust collection bucket taken out of the larger bucket. Residual dust was rinsed into the dust collection bucket and the rinsate was poured into a sample bottle for filtering and weighing in the lab. The timing of sampling varied by location and date (Table 1.0).

Table 1.0 Sampling dates at each location. * Letters indicate the sampling interval and type of traffic: a. sampled three times, each after 20 passes of a pickup truck, b. sampled initially for ambient traffic, then sampled three times after 20 passes of a pickup truck, and c. ambient traffic only.

Chi Road 1	Chi Road 2	Mid Pines Road
9/18/2019a*	11/6/2019a	9/4/2020c
9/19/2019b	11/7/2019b	9/13/2020c
9/24/2019b	11/13/2019c	9/20/2020c
10/1/2019c	11/20/2019c	9/28/2020
10/9/2019c		10/2/2020c
10/15/2019c		10/15/2020c
		10/23/2020c

Three products were tested to represent three different chemistries and methods for dust control, as mentioned in the Introduction. The polyvinyl acetate and polyacrylamide were applied according to the manufacturer’s recommend rate and method. The CaCl₂ was applied according to the recommendation provided in a fact sheet (Vermont Local Roads Program, undated) and

the American Association of State Highway and Transportation Officials Maintenance Manual (1976). Details are provided in Table XX. The products were applied late in the day and allowed to dry overnight before dust sampling was initiated on Chi Road. Sampling at Mid Pines Road started a week after the products were applied. Also, CaCl₂ was still evident at the second Chi Road test so no new product was applied.

Table 1.1 Dust control products used in the study, with application rate and method.

Product	Manufacturer	Application Rate	Application Method
Calcium Chloride Pellets	Occidental Chemical Corporation	100lbs/1000ft ²	Push type fertilizer spreader
Dust Down Poly Pro (polyvinyl acetate)	Factory Direct Chemicals	5 gallons of concentrate mixed with 100 gallons of water, and sprayed out at a rate of 40 gallons per 1000ft ²	Hydro Seeder
Granular H30 PAM (polyacrylamide)	Carolina Hydrologic	2 lbs of PAM dissolved in 300 gallons of water and sprayed out at 69 gallons per 1000 ft ²	Hydro Seeder

Table 1.2 Rainfall during or between the dust monitoring periods.

Chi Road 1 9/17/2019 to 10/15/2019		Chi Road * 10/15/2019 to 11/5/2019		Chi Road 2 11/5/2019 to 11/20/2019		Mid Pines Road 8/26/2020 to 10/23/2020	
Date	Rainfall l (inches)	Date	Rainfall l (inches)	Date	Rainfall l (inches)	Date	Rainfall l (inches)
10/13/2019	0.73	10/16/2019	0.40	11/8/2019	0.27	8/29/2020	0.08
		10/20/2019	1.41	11/12/2019	0.89	8/31/2020	4.25
		10/27/2019	0.23	11/15/2019	0.43	9/8/2020	0.09
		10/30/2019	0.32	11/18/2019	0.18	9/9/2020	0.11
		10/31/2019	0.46			9/11/2020	0.80
						9/18/2020	1.92
						9/25/2020	1.27
						9/29/2020	1.43

						10/11/202	
						0	1.22
						10/16/202	
						0	0.76
Total	0.73		2.82		1.77		11.93

*Between monitoring periods

Results and Discussion

The first testing on Chi Road happened to be a relatively dry period, with only one rain event four days before the last samples were collected. This was the only test in which we included water as a dust control treatment, mimicking what is typically done on construction sites by spraying water from our hydroseeder onto the road. The effect was evident briefly on the first day after application but was gone by the next day (Figure 1.8). Both the polyvinyl acetate and CaCl₂ reduced dust substantially immediately after treatment, but the effect was less evident two days and a week after treatment. However, the CaCl₂ effect rebounded to around 50% dust reduction over the next few weeks and declined at the last sampling, a month after application. The polyvinyl acetate effect was relatively small (<20% reduction) after the first day.

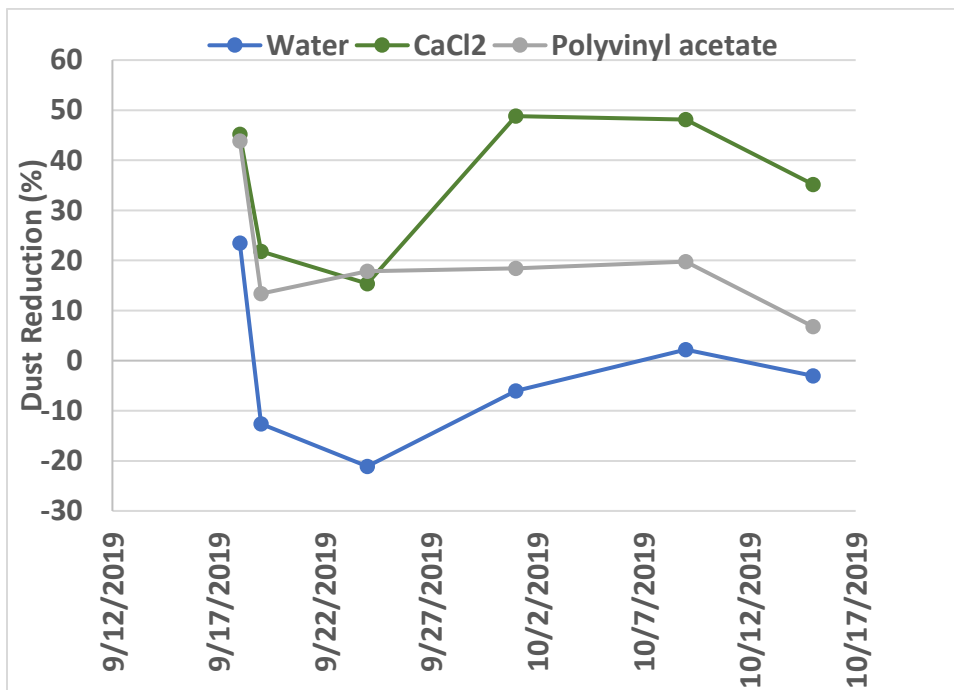


Figure 1.8 Dust reduction for treatments on Chi Road as a fraction of the untreated control during the first test period. One rain event of 0.73” occurred on 10/13.

After nearly a month, a second test period was initiated on the same sections of Chi Road. Approximately three inches of rain fell during this period. The polyvinyl acetate treatment was applied to the same sections where it had been applied earlier. The sections that had been watered received a treatment of dissolved polyacrylamide. Because the CaCl_2 treatment was still evident as moisture in the treated sections, no additional application was made. The polyvinyl acetate continued to have minimal effect, with a high of 28% reduction in dust (Fig. 1.9). The polyacrylamide section had little dust reduction initially, and actually had much more dust than the control in the last two sampling periods. The CaCl_2 initially reduced dust by around 40%, but this dropped to <20%

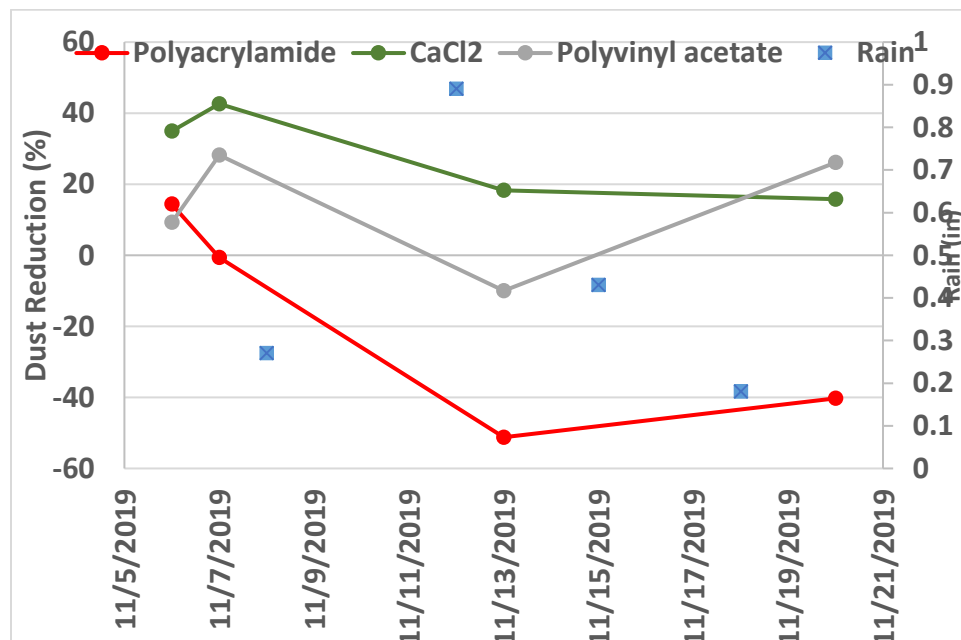


Figure 1.9 Dust reductions for treatments on Chi Road as a fraction of the untreated control during the second test period.

A third test was conducted on a different gravel road on the research station, Mid Pines Road. This road has considerable vehicular traffic due to its convenience as a short cut between Tryon Road and Lake Wheeler Road. We installed a game camera to gauge traffic and found that approximately 1,000 vehicles traverse this road per week. We did not do any simulated traffic due to the ambient traffic. This testing period was much wetter than the others, with nearly 12” of rain during the sample collection. Again, only the CaCl_2 provided consistent reductions in dust control, ranging from 15% to 59% reduction (Fig. 1.10).

Conclusions

It was known from field experience that the effect of water on dust control during warmer times of the year is very short lived, often less than a few hours. Neither of the “glue” type products, polyvinyl acetate and polyacrylamide, were effective dust control agents under these conditions. They may be more appropriate in untrafficked areas, although these generally are not generating significant dust in our region. CaCl_2 was fairly consistent in reducing dust by 30-40% over many

weeks of testing, and this might be improved if it was added in solution and mixed into the surface several inches, as several publications suggest.

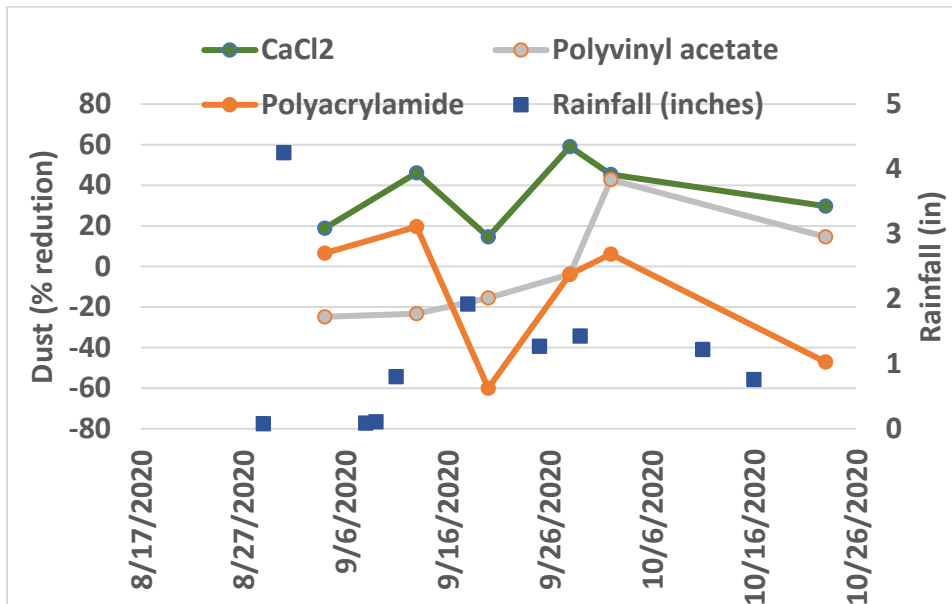


Figure 1.10 Dust reduction for treatments on Mid-Pines Road as a fraction of the untreated control section.

Literature Cited

Cruzer, J., C. L. M. Hargiss, J. E. Norland, T. DeSutter, F. X. Casey, E. S. DeKeyser, and M. Ell. 2016. Does increased road dust due to energy development impact wetlands in the Bakken Region? *Water Air Soil Pollut* 227(1): 1-14.

Johnson, E. N., and R. C. Olson. 2009. Best Practices for Dust Control on Aggregate Roads. MN Department of Transportation. <https://www.lrrb.org/pdf/200904.pdf>.

Jones, D., A. Kociolek, R. Surdahl, P. Bolander, B. Drewes, M. Duran, L. Fay, G. Huntington, D. James, C. Milne, M. Nahra, A. Scott, B. Vitale, and B. Williams. 2013. Unpaved Road Dust Management, A Successful Practitioner's Handbook. Federal Highway Agency Report FHWA-CFL/TD-13-001. https://www.fhwa.dot.gov/clas/ctip/unpaved_roads_dust/

Sanders, T.G., Addo, J.Q., Ariniello, A. and Heiden, W. 1997 Relative Effectiveness of Road Dust Suppressants. *Journal of Transportation Engineering, ASCE*, September 1997, pg.393-397.

Chapter 2: UAV Applications on Construction Sites

Introduction

During World War II, unmanned aerial vehicles (UAVs) were used for remote surveillance to prevent soldiers from exploring high-risk areas (Eisenbeiss et al. 2004). Currently, UAVs are being used in different sectors, such as agriculture, disaster management, and construction (Zhao and Borakdarpour, 2018). Also, Zhao and Borakdarpour (2018) reported that the construction industry uses UAVs equipped with thermal, hyperspectral, and regular cameras to increase project management productivity. UAVs equipped with regular cameras can collect images with photogrammetric software to produce three-dimensional models to illustrate the progression of a project (Feng et al., 2015). Kim et al. (2017) used computer algorithms and images acquired by UAVs to determine potential risks of equipment to improve workers' safety. Dorafshan and Maguire (2018) reported that US states have used UAVs to detect structural issues in bridges, allowing them to save time and labor compared to traditional bridge evaluations.

UAVs can also be usefully applied in the civil engineering industry, but there is limited research on how they can *assist* inspectors with E&SC. Perez et al. (2015) and Kazaz (2019) have shown that UAVs are capable of detecting E&SC device issues and have suggested that these are accurate and less time consuming than regular on-site inspections. Nevertheless, these and other studies do not provide enough information to validate whether UAVs can detect a variety of E&SC devices while saving time during site evaluation.

Under the Clean Water Act of 1972, the national pollutant discharge elimination system (NPDES) regulates point and nonpoint pollutant sources. The NPDES states that construction

operators must apply for a construction general permit (CGP) if the land disturbance is larger than one acre (United States Congress, 2002). Furthermore, the NPDES program requires erosion and sediment control (E&SC) measures to limit erosion during land disturbances and grading activities on construction sites in the US (USEPA, 2017). Although the CWA is a federal regulation, each US state can create its own NPDES program. For example, North Carolina, which is the location of this study, established an NPDES program, amended to the North Carolina Sediment Pollution Control Act of 1973, consisting of E&SC plans approved by the Department of Environmental Quality (or a delegated program) to mitigate erosion (NCGA, 2002).

The North Carolina Department of Transportation (NCDOT) enforces this plan in their projects by maintaining or operating activities that reduce sediment loss. Companies contracted through this NCDOT must use preventive measures – including erosion controls, stream diversions, buffers to protect jurisdiction surface waters, ground stabilization, management of the work area, and site clean-ups – to reduce sediment loss. Furthermore, to comply with CGP guidelines, regular on-site inspections and documentation must be completed by a qualified inspector to identify E&SC or stormwater device issues (USEPA 2017). The inspector must review unstable sites at least once weekly or within 24 hours if more than 1 inch of precipitation occurred at the site. Any routine corrective action deemed urgent by the inspector needs to be addressed within 24 hours of the inspection. If not urgent, the routine action must be completed within five days. However, a traditional on-site inspection is time-consuming and hazardous when walking or driving on rugged terrain or after rains.

To investigate the potential use of UAVs for weekly site inspections, this study responds to two questions: (1) How do UAVs and traditional on-site inspections compare in finding E&SC

device issues on construction sites? (2) Do manual or autonomous UAV inspections save more time than conventional on-site inspections?

In addition, we were interested in determining the accuracy of UAV point locations as affected by the UAV equipment used and how the data was collected and processed. Two questions were posed to evaluate this: (1) What are the differences in accuracy of surveys conducted by UAVs equipped with either a consumer-grade GPS or one with more advanced technology (RTK), either with or without correction based on ground control points? (2) What are the effects on accuracy of image overlap, height, and distribution and quantity of GCPs on both types of UAV technology?

Geographic information systems (GIS) can be used to develop a digital elevation model (DEM) base on images obtained through the UAV. These can help civil designers implement the best erosion and sediment control (E&SC) practices, based on hydrologic analysis. This procedure can help identify areas susceptible to erosion and runoff and potential failure points. Further, GIS analysis can measure sediment removal or deposition using DEM. Overall, this part of the study had two objectives: (1) Determine volumetric changes over time for a borrow pit (2) Conduct hydrologic analysis to determine the performance capacity for E&SC devices based on the delineation of watersheds and flow patterns.

Materials and Methods

Study Sites

Two road construction sites were selected, one at NC Highway 42 East in Clayton, NC, and the other at US-401 in Youngsville, NC, which are two road-widening projects (Figs. 1.1-1.2). The total length for both sites was beyond the ability of the pilot to maintain visual contact with the UAV, thus the projects were broken up into three sections, so the pilot could move to each section while still being able to see the device. The first section for NC Highway 42 East had an estimated area of 3.4 ha. The second section was 9.2 ha, while the third was 10.3 ha. Approximately, the first section for NC Highway 42 East had 115 erosion and sediment control measures (E&SCs). The second section had 304 E&SCs, while the third contained 436 E&SCs. The US-401 sections were 10.1 ha, 15.5 ha, and 13.8 ha. Also, the sections had roughly 237, 162, and 295 E&SCs.

Inspection Testing

Weekly on-site inspections were conducted in both sites to identify any E&SC failures. A stopwatch was used to record how long it took to inspect each section. Furthermore, a field book was used to note where an E&SC failure occurred at a location. It was essential to consider different factors when evaluating the respective site: the time needed to move from one road to another; the time needed to move from one section to another via vehicle; the time needed to walk back to the vehicle after completing an inspection; the actual time needed to conduct inspections. These considerations were considered when calculating the average time needed to fill out an official NPDES inspection form.

DJI Phantom 4 RTK (PRTK; DJI, Shenzhen, China) was used to inspect sections manually using its remote control to operate the UAV. When inspecting a section, the PRTK collected images using a 4:3 aspect ratio and flying at a minimum elevation of 37m at both sites to avoid cranes, power lines, and trees. The erosion control plans for both sites were used to locate the

practices where issues were identified by the manual UAV inspections and those identified by the conventional on-site evaluations.

When conducting the manual UAV inspection, there were several steps which were included in the total time for the inspection. These included the time needed to collect images when operating the PRTK; the time needed to review images acquired from the UAV and fill out any issues onto an official NPDES inspection form; the time needed to conduct pre-flight inspections; the time needed to move from one section to the other by vehicle; the time needed to download images from the micro-SD card onto the computer. These steps were summed to obtain the final amount of time needed to conduct this type of inspection.

In this study, DJI Mavic Pro Platinum was used to conduct autonomous UAV inspections (MPP; DJI, Shenzhen, China). MPP with the use of DJI GS Pro (DJI, Shenzhen, China), an application that can create autonomous flight missions through a tablet device using waypoints, photographed sections autonomously. Although the remote controller of the PRTK can create autonomous flight missions, the objective of using this application was to see if there is a cheaper option available to inspectors. Waypoints are points created using the DJI GS Pro that signal to the GPS receiver of the UAV where the UAV should operate. All points can have the same settings, which include the same elevation, camera angle, whether to take pictures or videos, or how long to hover at a specific location. For the autonomous flight missions, the DJI GS Pro configured the PRTK using different elevations of 37m, 60m, and 120m with a camera angle set at 55° or 90°. This was done to see if altitude or camera position affects UAV inspections when taking pictures or videos. The aspect ratio for the images was 4:3, while the video frame had a 1920x1080 frame. The aspect ratio for the video was a different size to ensure it could obtain adequate site coverage while nonetheless having enough memory space for the

micro-SD card to inspect multiple sections. Similar erosion control plans were used as the manual UAV inspection, and the same factors had to be considered during the autonomous flights when evaluating sites. Furthermore, the time to create a flight mission for the UAV was another factor to include when conducting this type of inspection for both image and video treatments.

UAV Accuracy Determination

Ground control points (GCPs) were located using an Emlid RS 2 (Emlid, Hong Kong, SAR, China), a handheld GPS receiver using RTK technology. A one-time access cost was paid to access North Carolina GNSS Real Time Network (RTN) to test and verify the accuracy of the receiver. Manufacturer claimed accuracy is centimeter-level when in RTK mode. In addition, additional GCPs were located by a private firm as part of the NCDOT project, using Trimble R10 GNSS-Receiver (Trimble Inc, Sunnyvale, CA). The two UAVs tested were a Mavic Pro Platinum (MPP) and Phantom 4 RTK (PRTK) (DJI, Shenzhen, China). The technical specifications for the MPP and PRTK UAVs are provided in Tables 2.0 and 2.1, respectively.

Table 2.0. Camera and technical specifications on how Mavic Pro Platinum operate.

Satellite Positioning Systems	GPS / GLONASS
Max Flight Time	Roughly 27 minutes
Max Service Ceiling Above Sea Level	16404 ft (5000 m)
Operating Temperature	32° to 104° F (0 to 40°C)
Sensor	Effective pixels:12.35 M
Lens	FOV 78.8° 26 mm (35 mm format equivalent) f/2.2 Distortion < 1.5% Focus from 0.5 m to ∞
Image Size	4000×3000
Electronic Shutter Speed	8s -1/8000 s
Iso Range	photo: 100-1600
Supported SD Cards	Micro SD™ Max capacity: 128 GB

Table 2.1. Camera and technical specifications of how Phantom 4 RTK operate.

Satellite Positioning Systems	Single-Frequency GNSS, Multi-Frequency RTK GNSS
Max Flight Time	Roughly 30 minutes
Max Service Ceiling Above Sea Level	19685 ft (6000 m)
Operating Temperature	32° to 104° F (0° to 40° C)
Sensor	Effective pixels: 20 M
Lens	FOV 84° ; 8.8 mm / 24 mm (35 mm format equivalent:24 mm); f/2.8 - f/11, auto focus at 1 m - ∞
Image Size	4864×3648 (4:3); 5472×3648 (3:2)
Electronic Shutter Speed	8s -1/8000 s
Iso Range	Photo: 100-3200(Auto)
Supported SD Cards	Micro SD™ Max capacity: 128 GB

Within the designated section of NC Highway 42 East, six out of the fourteen points represented locations that NCDOT surveyed by using Trimble R10 GNSS-Receiver. These locations established for the NCDOT project were imported in a .kml file spatially referenced to the North Carolina state plane coordinate system, NAD83, feet (EPSG 2264). To help identify these staked locations in the aerial images, 4" x 4" plywood squares were painted and placed over the stakes. For comparison, these points were also located using our RTK-GPS (Emlid RS 2) with data collection times of 40 seconds (40 points) and 5 minutes (300 points). An additional eight North Carolina State University (NCSU) GCPs were established elsewhere on the site using the Emlid RS 2 unit, with collection times of 40 seconds. These GCPs were identified with 2' x 2' Sky High Bull's-Eye ground control points (Willis Worxs LLC, Birmingham, AL). These markers were placed along the corridor and spaced within thirty meters of NCDOT points. Similarly, a distribution of nineteen 2'x 2' Sky High Bull's-Eye ground control points identified as NCSU were located around the boundary and interior of the borrow pit. The RTK-GPS (Emlid RS 2) located each GCP at 5-minute intervals. After the conclusion, locating GCPs at 40 seconds

or 5 minutes acquired similar positioning measurements based on NC Highway 42 East time intervals.

Flight Missions

At NC Highway 42 East, both UAVs were flown at 60 m and 120 m and the flights were configured to collect images using either 20% (front) x 20% (side) overlap or 75% (front) x 60% (side) overlap to acquire images automatically (Table 2.2). Only the MPP surveyed the borrow pit using one elevation at 80m and overlap at 75% (frontal) x 60% (side). The MPP remote control software resides on a smartphone (or tablet) and can be used for mission setup and real-time display. Pix4Dcapture (Prilly, Vaud, Switzerland), was used to create flight missions in the flight controller software. In contrast, the Phantom 4 RTK has its own remote control which includes a touch display and software capable of visual or manual set-up of flight missions. RTK corrections from the North Carolina Real Time Network (RTN) were obtained using a personal WiFi hotspot and corresponding cellular data plan (AT&T, Dallas, TX, USA).

Table 2.2 Flight mission settings that were conducted on NC 42 East’s section 1.

Flight #	UAV	Elevation (m)	Overlap (%)	Images
Flight 1	MPP	60	20x20	35
Flight 2	MPP	60	75x60	310
Flight 3	MPP	120	20x20	29
Flight 4	MPP	120	75x60	122
Flight 5	PRTK	60	20x20	50
Flight 6	PRTK	60	75x60	332
Flight 7	PRTK	120	20x20	41
Flight 8	PRTK	120	75x60	194

Obtaining True Elevation for Real Time Kinematic- Global Positioning System Points

Elevation for each RTK-GPS point needed correction by including respective geoid and initial heights to obtain true vertical representation. Horizontal Time-Dependent Positioning (HTDP), a database from the National Oceanic and Atmospheric Administration (NOAA) transformed RTK-GPS points initially from the WGS 84 frame to coordinates based of the fixed North American plate. These converted coordinates are inserted in, Geoid12B, a system of NOAA which is used by NCDOT to determine geoid elevations were applied to each RTK-GPS point.

Photogrammetric Software: Agisoft Metashape

The following describes the process of how the photogrammetric software, Agisoft Metashape version 1.5 (Agisoft LLC, St. Petersburg, Russia) produced these digital surface models (DSMs) and orthomosaic (Agisoft, 2018). Images collected by both UAVs were stitched together by implementing structure from motion (SfM) created spatially referenced orthomosaics and digital surface models. The first step was the alignment of images. This procedure used the camera position of each image to generate a sparse cloud (an unrefined model of 3D point clouds), essentially a rough estimate of the model. The photogrammetric software refined the model by using GCPs.

Re-projection functions in ArcGIS version 10.6.1 (ESRI, San Diego, CA) were used to transform NCDOT points' measurements to WGS 84 coordinates to match RTK-GPS locations and image positions received from the respective UAV GNSS (WGS 84). The imported GCPs were used to help refine the DSM by reducing georeferencing errors. A separate set of GCPs was used as checkpoints as an accuracy assessment of the model. The optimization procedure realigned the estimated coordinates for the cameras and markers to minimize georeferencing

errors. Once completed, a dense cloud (a refined model of 3D point clouds) was created, with DEMs and orthomosaic images created from the dense clouds.

Ground Control Points and Checkpoints Treatments

The effects of GCPs, overlap, elevation, and UAV on the precision of the DSM and orthomosaic were tested by running the image processing software with all combinations of these factors. During this workflow, the DSMs and orthomosaics for NC Highway 42 East were generated using four different levels of GCP correction: no GCPs, six NCDOT GCPs, eight North Carolina State University (NCSU) GCPs, and all 14 GCPs. These were run with data from each UAV at each elevation and overlap amount. Only one level of applied GCP correction regarding the borrow pit used nine of the nineteen ground control points for the photogrammetric procedure.

Calculating Image Accuracy

The default WGS 84 coordinates for both digital surface model and orthomosaic are converted to EPSG 2264 when exported to ArcGIS. ArcGIS acquired computational horizontal measurements based on the respective checkpoints within orthomosaic while vertical positions obtained from the DSM. However, to compare horizontal position between NCDOT survey coordinates and RTK-GPS points. ArcGIS used re-projection functions to transform collected RTK-GPS (Geographic coordinates- WGS84) data into North Carolina state plane coordinate systems (EPSG 2264). Regarding digital surface model, the layer was placed on top of orthomosaic to determine vertical measurement based on respective checkpoints. The difference in coordinates between computational and GNSS “surveyed” resulted in the horizontal and vertical root mean square errors (RMSE) for the following treatments.

Digital Surface Modelling, Orthomosaic Creation, and Accuracy

The use of photogrammetric software and ground control points was necessary to create georeferenced DEMs and orthomosaics. The Agisoft Metashape version 1.5 software (Agisoft LLC, St. Petersburg, Russia) implemented structure from motion (Sfm), a technique that applies computational logarithms and alignment of image positions obtained from Mavic Pro Platinum. A detailed explanation regarding the borrow pit and NC Highway 42 East accuracy is in the previous chapter.

ArcGIS Applications on Digital Surface Models

High resolution DEMs obtained from photogrammetry applications can act as a base to conduct hydrologic analysis. The hydrology toolset with ArcGIS version 10.6.1 (ESRI, San Diego, CA) has multiple procedures to estimate surface water flow and delineate watersheds. The fill tool eradicated any sinks (depressions) within the DEMs. The flow direction tool calculated water direction from every raster cell based on the fill layer and Deterministic 8 (D8) procedure. Kiss, Richard (2004) explains that the D8 application is a standard GIS procedure that uses slope value within a cell to determine eight possible flow directions, moving to adjacent cells. The flow accumulation tool created a raster flow calculated from the accumulated weight of each cell based on D8 measurements. Within the software, the raster calculator filtered certain accumulated flow values to zero or one. The purpose was to classify water flows. Point features were created to show where computed water flow will enter E&SC devices within the site. The watershed tool delineated watershed areas based on flow direction values near point features. The conversion tool converted watersheds into vectors to determine area and changed water flows that were classified as one into polylines. The inclusion of contours and orthomosaics

illustrated where computational water will flow. ArcGIS applications can also determine elevation change based on DEMs.

DEMs developed over time can measure soil deposition and removal within the borrow pit. The raster calculator measured elevation change by subtracting the values between two DEMs. Each DEM difference layer had to be classified by altering the symbology property, excluded elevation values caused by non-terrain obstacles, and arranged values to represent sediment deposition and removal. Point features outlined sections of net changes between DEMs using field geometry to measure deposition and excavation areas. The zonal statistics tool averaged raster cell values within the outlined zones while using the DEM difference layer as the base. The averaged value represented depth for each zone; this was multiplied by the respective deposition and removal area to obtain volume measurements. Also, volume measurements obtained from multiple DEM differences were compared to NCDOT estimates acquired by trucks with 11m³ (14 cubic yard) capacity, a standard procedure within the civil engineering sector uses truck dimensions to record net changes (NCDOT, 2012).

Drainage Area Changes Over Time

Drainage area values were compared between computation and the design to determine whether these the drainage areas were within the design for each device. Each respective basin and sediment fence outlet had its delineated watershed measured by computational measures within ArcGIS to obtain area. Equation 2.1 used basin designs to achieve real-life capacity. The combination of equations 2.2 shows storage volume towards sediment fence sections concerning both NCDOT designs and ArcGIS measurements.

$$\text{Eq. 2.0 } (Length (m) \times Width (m) \times Height (m)) \div 51m^3$$

$$= \text{Drainage Acreage for respective basin}$$

$$\text{Eq. 2.1 } (Sediment Fence Length (m) \div 30m) \times .25ac$$

$$= \text{Drainage Acreage for respective sediment fence}$$

Results

The accuracy of both vertical and horizontal point locations was greatly improved when ground control points were included at both elevations for the MPP, but not for the PRTK (Figs. X and Y). With the GCP correction, the MPP had similar accuracy to the PRTK. This suggests that a calculation could be made to determine if the additional cost of the PRTK could be justified based on time savings in establishing GCPs and correcting the data, which would not be necessary. The MPP vertical accuracy was better at the higher elevation (120 m) and horizontal accuracy better with more overlap, but both effects were eliminated when GCPs were used to correct the data.

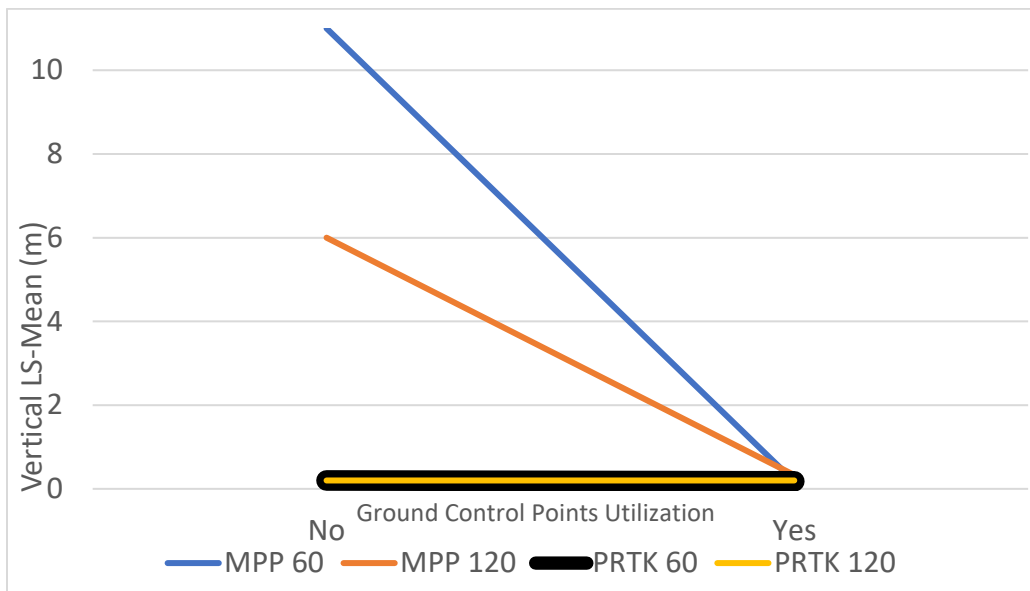


Figure 2.0 The effect of using ground control points to correct vertical accuracy for the MPP and PRTK UAVs at 60 m and 120 m.

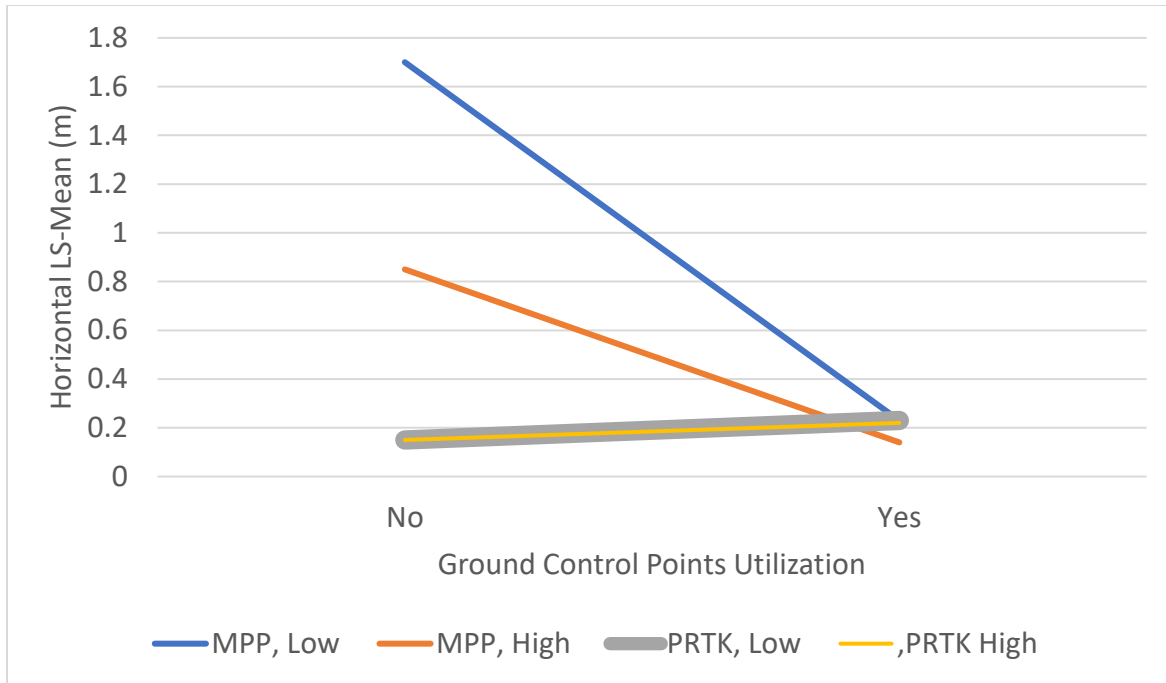


Figure 2.1 The effect of overlap and ground control points on horizontal accuracy for the MPP and PRTK UAVs at 60 m and 120 m.

The number of GCPs needed was also evaluated at both the NC 42 and the borrow pit sites. The sites had 14 (NC 42) and 19 (borrow pit) GCPs established, but the MPP only needed about half of those numbers to achieve centimeter accuracy, and adding more points also did not improve accuracy. When establishing GCPs using GPS-based instrumentation, we also found that collecting data at a point for five minutes did not improve accuracy over 40 s data collection. We did not determine a minimum amount of time needed beyond which the accuracy was not improved.

Inspections Comparison

At the NC Highway 42 East site, both inspection methods produced similar problem detection rates for most of the BMPs (Table 2.3). The UAV detected more issues with rock inlet protection, and to a lesser extent rock check dams. This suggests there may be an advantage to seeing these features from above. However, on-foot inspections found more issues with silt fences. Silt fence issues were also more likely to be detected by on-foot inspections at US 401 (Table 2.4). While serious breaches could be detected from UAV pictures, tears and minor undercutting were more difficult to see in aerial pictures compared to in-person inspection.

Table 2.3 Comparison of problem detections by either UAV or on-foot inspections of nine common BMPs on the NC 42 site.

Erosion and Sediment Control Device	Total Detected	Detected by both by both or UAV only	Detected by both by both or on-site only	p-value	Common Issue(s)
		Percent (%)			
Baffle	13	92	75	0.3	<ul style="list-style-type: none"> • Damaged because of object
Geotextile Fabric	6	67	100	.	<ul style="list-style-type: none"> • Tears • Not properly installed
Inlet Protection	14	57	100	.	<ul style="list-style-type: none"> • Sediment deposition • Clogged Slope Drain
Rock Check Dam	37	90.6	81.3	0.06	<ul style="list-style-type: none"> • Sediment deposition
Rock Inlet Protection	13	92	46	0.03	<ul style="list-style-type: none"> • Sediment deposition
Rock Lined Ditch	25	92	84	0.4	<ul style="list-style-type: none"> • Sediment deposition
Silt Fence	16	25	81	0.02	<ul style="list-style-type: none"> • Sediment deposition • Tears
Special Sediment Control Fence	15	53	67	0.6	<ul style="list-style-type: none"> • Sediment deposition
Wattle	13	100.0	62	.	<ul style="list-style-type: none"> • Sediment deposition • Undermining

Table 2.4 Comparison of problem detections by either UAV or on-foot inspections of nine common BMPs on the US 401 site.

Erosion and Sediment Control Device	Total Detected	Detected by both by both or UAV only	Detected by both by both or on-site only	p-value	Common Issue(s)
		Percent (%)			
Baffle	3	100.0	80.0	NA	<ul style="list-style-type: none"> • Damaged because of object
Geotextile Fabric	4	75.0	100.0	NA	<ul style="list-style-type: none"> • Sediment deposition
Inlet Protection	16	63	93	0.6	<ul style="list-style-type: none"> • Clogged Slope Drain • Poor Drainage
Rock Check Dam	13	85	77	0.7	<ul style="list-style-type: none"> • Sediment deposition
Rock Inlet	3	100.0	100	NA	<ul style="list-style-type: none"> • Sediment deposition
Rock Lined Ditch	3	100.0	100	NA	<ul style="list-style-type: none"> • Sediment deposition
Silt Fence	13	23	92	0.01	<ul style="list-style-type: none"> • Sediment undercut • Weakened fabric
Special Sediment Control	7	43	57	0.7	<ul style="list-style-type: none"> • Sediment deposition • Rusted steel mesh

The amount of time it took to conduct inspections and fill out the required forms by UAV and on-foot was compared for three sections each at NC 42 and US 401. At NC 42, the UAV method took an average of 17 minutes less time (Table 3.5). Some of the difference was in the approach of the inspector at that site, who did the physical inspection and took notes but filled out the forms back at the office. At the US 401 site, only on one section was the UAV method faster, but it was 10 minutes faster overall (Table 3.6). There may have been an area factor, with the UAV method saving more time the larger the section. Examples of failures found in images collected by the UAV are shown in Figures 2.2 – 2.4.

Table 2.5 Comparison of time required to conduct inspections at the NC 42 site. Negative values indicate on-foot was faster, positive that UAV was faster.

Section	Size (ha)	Degree of Freedom	t-Value	Mean Difference (min)	P-value
1	4.2	10	2.2	4	0.03
2	9.2	19	4.0	23	0.0003
3	10.3	11	3.4	23	0.003
All Sections		51	3.8	17	<0.0001

Table 2.6 Comparison of time required to conduct inspections at the US 401 site. Negative values indicate on-foot was faster, positive that UAV was faster.

Section	Size (ha)	Degree of Freedom	t-Value	Mean	P-value
1	10.1	6	1.8	9	0.1
2	15.5	6	2.5	18	0.05
3	13.8	6	0.78	5	0.5
All Sections		22	2.7	10	0.01



Figure 2.2 Example of a wattle failure with undercutting and ditch erosion at the NC 42 site.



Figure 2.3 Example of baffle failure due to placement of a slope drain on top of the baffle.



Figure 2.4 Example of heavy sediment deposition on one side of a Type C Rock Inlet Protection device.

UAV Use for Landscape Analysis

There were two objectives in developing digital elevation models (DEMs) from UAV images. The first was to estimate volume changes at the site as borrow was removed or stockpiled. This

could be useful as an alternative to counting trucks or other methods, as it is relatively easy to fly the site periodically. The second objective was to estimate drainage areas for sediment basins and silt fences. This would provide a mechanism for alerting site managers when the drainage area exceeds the design specifications for a device.

The borrow pit was flown four times from late January to June of 2020 and DEMs were developed to determine the changes in elevations over the site. An example is shown in Figure 2.5 for the period from March 23 to June 12, 2020. The changes in the landscape, either positive or negative for excavated and stockpiled areas, respectively, were calculated for each period (Table 2.7). The level of activity varied considerably over the six months of UAV surveying. The DEM estimates were reasonably close to the truck count estimate, with a difference of 5.6% over the period.

The borrow pit site had five sediment basins and seven sections of silt fence, each of which had a special silt fence (gravel) outlet at the low point. At no point in the six months of our surveys did the drainage area exceed the design of the sediment basins (Table 2.8). At one point Basin 1C had about 70% of the design drainage area, but in most cases the drainage areas were a much smaller fraction of the design. In contrast, the sediment fence sections sometimes had drainage areas as much as four times the design for them (Table 2.9). This varied considerably as a result of elevation changes due to site grading activity. However, there was no evidence that there was overloading and failure at any of the sediment fence sections. The flow analysis did show flow through a diversion at Basin 1D (Figure 2.7), and an inspection on the ground did find a breach in the diversion (Figure 2.8).

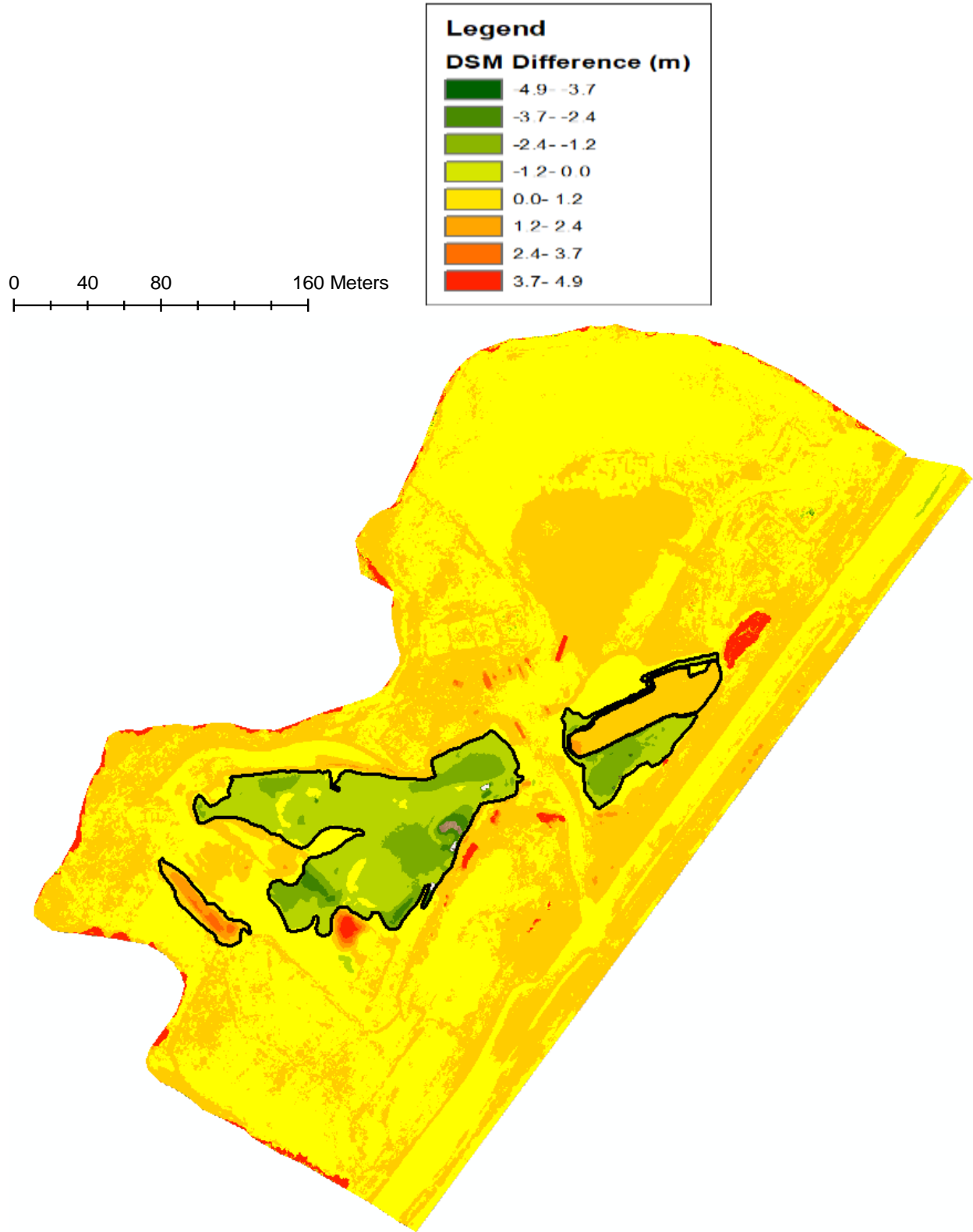


Figure 2.5 Elevation changes at the borrow pit from March 23 to June 12, 2020.

Table 2.7 Volume changes at the borrow pit at US 401 over different time intervals, as estimated by DEMs developed from UAV images or by counting trucks (NCDOT).

Date (Timeframe)	UAV Estimates		NCDOT Estimates	
	Excavation	Deposition	Net	Export
01.28.20- 03.09.20	6390	2195	4195	4644
03.09.20- 03.16.20	5485	0	5485	6028
03.16.20- 03.23.20	980	0	980	719
03.23.20- 06.12.20	27046	2380	24666	22064
Total Sum	39901	4575	35326	33455

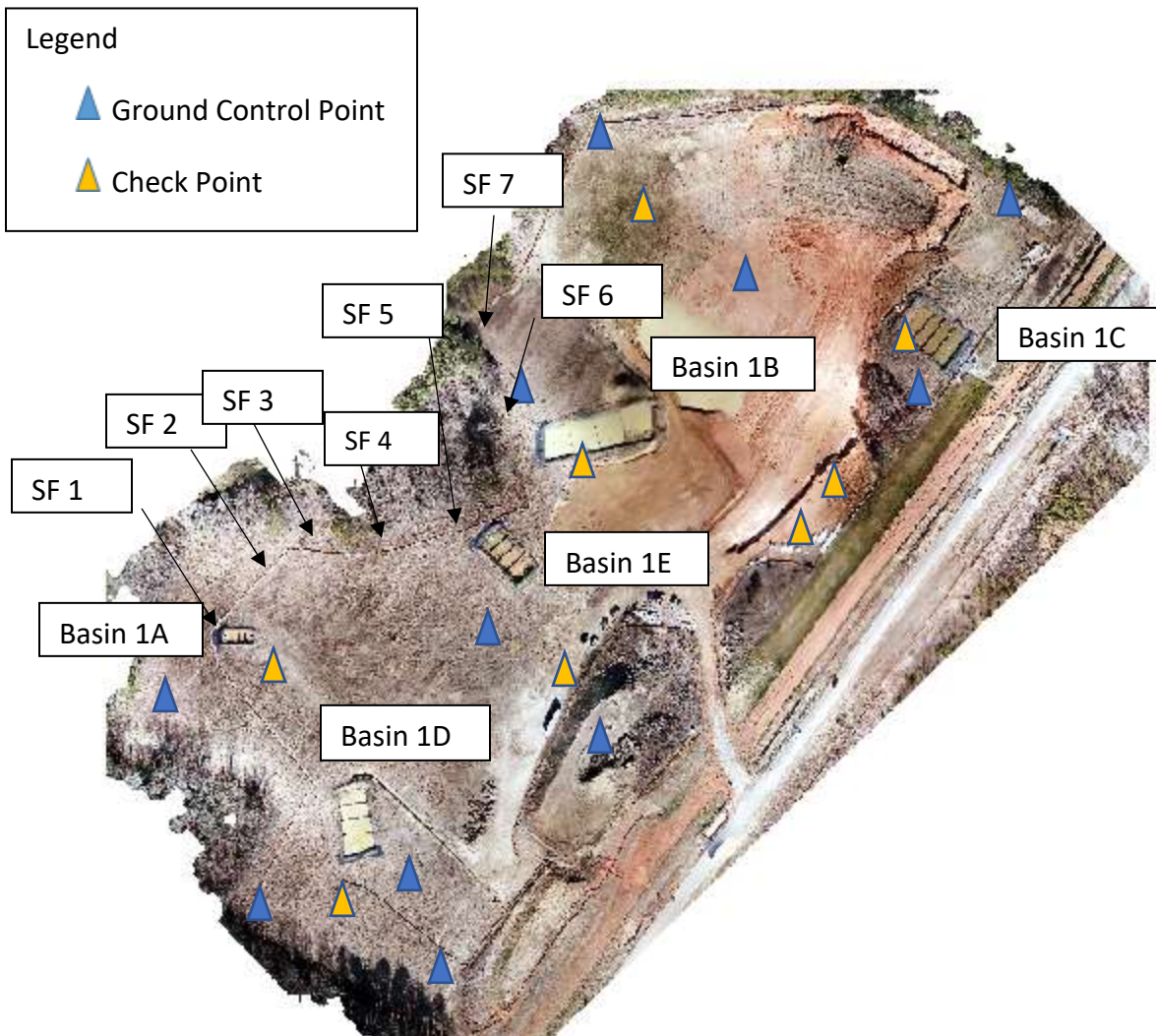


Figure 2.6 US 401 borrow pit area showing locations of various sediment basins and silt fence outlets (SF). The ground control and check points were used to determine the accuracy of locations by the MPP (discussed earlier).

Table 2.8 Dimensions and estimated drainage areas at different survey dates for five sediment basins at the borrow pit site. Design drainage area is shown in parentheses below each basin designation.

Basin (ha)	1A * (0.8)	1B * (8.1)	1C * (5.7)	1D * (4.9)	1E * (3.2)
Dimensions (m)	(18 x 6 x 1)	(61 x 18 x 1)	(34 x 23 x 1)	(37 x 18 x 1)	(30 x 15 x 1)
Date	Estimated Acreage (ha)				
01.28.20	0.004	0.8	0.1	1.3	0.02
03.09.20	0.04	1.3	1.6	1.1	0.02
03.16.20	0.04	1.3	1.6	1.1	0.02
03.23.20	0.1	1.6	3.4	1.1	0.2
06.12.20	0.01	0.4	4.0	2.2	0.0

Table 2.9 Dimensions and estimated drainage areas at different survey dates for seven sediment fence locations at the borrow pit site. Design drainage area is shown in parentheses below each silt fence designation.

Sediment Fence (ha)	1 * (0.2)	2 * (0.2)	3 * (0.2)	4 * (0.1)	5 * (0.1)	6 * (0.3)	7 * (0.2)
Length (m)	59	55	58	41	41	83	50
Date	Estimated Acreage (ha)						
01.28.20	0.08	0.3	0.7	0.3	0.01	0.3	0.0
03.09.20	0.08	0.3	0.8	0.1	0.00	0.6	0.0
03.16.20	0.2	0.3	0.4	0.3	0.04	0.8	0.0
03.23.20	0.2	0.3	0.3	0.4	0.0	0.6	0.0
06.12.20	0.2	0.3	0.01	0.02	0.07	0.08	0.0

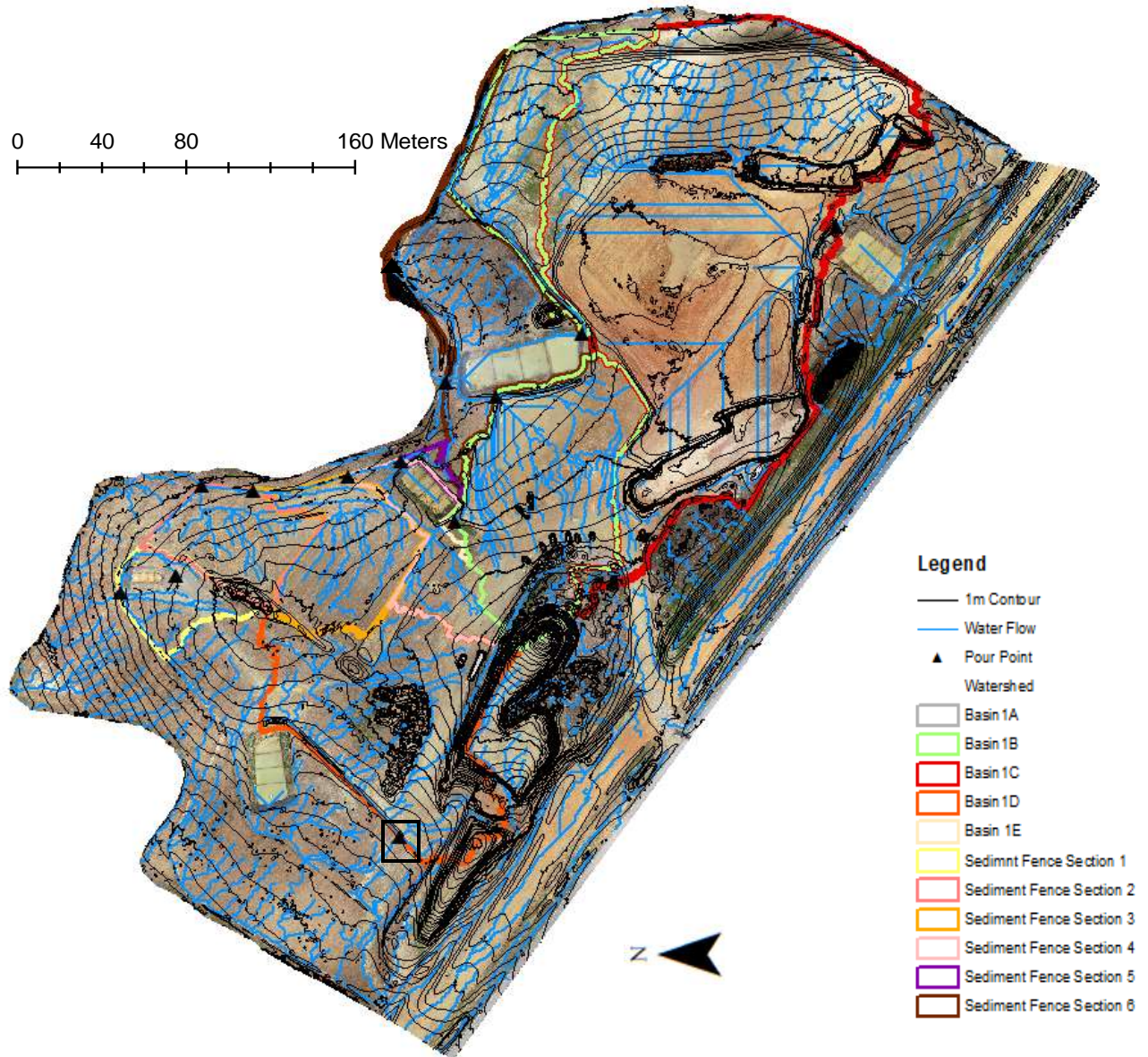


Figure 2.7 Watershed delineation of basins and sediment fence outlets as of 03.16.20 for US-401N borrow pit. The black rectangles are the inlets for the sediment basins and outlets for the sediment fence sections. The triangle in a square represents water flow breaching the diversion ditch for basin 1D. Contour lines represent elevation change from 113m to 117m.



Figure 2.8 Photo of the breach in the diversion for Basin 1D.

Literature Cited

- Cajzek, R., & Klanšek, U. 2016. An unmanned aerial vehicle for multi-purpose tasks in construction industry. *Journal of Applied Engineering Science*, 14(2): 314-327.
- Dorafshan, S., & Maguire, M. 2018. Bridge inspection: Human performance, unmanned aerial systems and automation. *Journal of Civil Structural Health Monitoring*, 8(3), 443-476.
- Eisenbeiss, H., Viswanath, P., Mathew, M., and Eisenbeiss, H. 2004. A Mini Unmanned Aerial Vehicle (UAV): System Overview and Image Acquisition ‘Processing and Visualization Using High-Resolution Imagery. *Heritage*, 36(5/W1), 1–9.

- Federal Aviation Administration. 2016. "Summary of Small Unmanned Aircraft Rule (Part 107)." (Part 107), 3. [Online]. https://www.faa.gov/uas/media/part_107_summary.pdf. Accessed December 02, 2020.
- Feng, Q., Liu, J., Gong, J. 2015. "UAV Remote Sensing for Urban Vegetation Mapping Using Random Forest and Texture Analysis." *Remote Sensing, Multidisciplinary Digital Publishing Institute*, 7(1), 1074–1094.
- Kazaz, B. 2019. Development of UAS-Based Construction Stormwater Inspections & Soil Loss Model. Master's Thesis, Iowa State University. Creative Components. 403. <https://lib.dr.iastate.edu/creativecomponents/403>
- Kim, D., Yin, K., Liu, M., Lee, S., & Kamat, V. R. 2017. Feasibility of a drone-based on-site proximity detection in an outdoor construction site. *Computing in Civil Engineering 2017* (pp. 392-400). American Society of Civil Engineers, Reston, VA, USA.
- NCGA. 2002. North Carolina General Statutes: Article 4, Chapter 113A. Sedimentation Pollution Control Act of 1973. Raleigh, N.C.: North Carolina General Assembly. https://www.ncleg.net/enactedlegislation/statutes/html/byarticle/chapter_113a/article_4.html. Accessed December 08, 2020.
- Perez, M. A., Zech, W. C., & Donald, W. N. 2015. Using unmanned aerial vehicles to conduct site inspections of erosion and sediment control practices and track project progression. *Transportation Research Record*, 2528(1), 38-48.
- United States Congress. 2002. "Federal water pollution control act." 33 U.S.C. 1251 et seq., 234." [Online]. <https://www.epa.gov/sites/production/files/2017-08/documents/federal-water-pollution-control-act-508full.pdf>. Accessed December 08, 2020.
- US Environmental Protection Agency. 2017. "Construction General Permit (CGP)." [Online]. https://www.epa.gov/sites/production/files/2019-05/documents/final_2017_cgpfact_sheet.pdf. Accessed December 08, 2020.
- Zhao, W., and Bonakdarpour, B. 2018. Decentralized Multi-UAV Routing in the Presence of Disturbances. arXiv preprint arXiv:1807.04823,1–10.

Chapter 3: Sediment Basin Hydrology

Materials and Methods

Data loggers with water level recorders and tipping bucket rain gauges were installed in the basins to be monitored. Onset Computer Corporation RX2104 data loggers with MX2001-04-S water level sensors and S-RGA-M002 rain gauges were used to get water level in the basin and rainfall on a 5 min interval. These devices were equipped with a cellular connection that allowed remote access to near real time data. There was also a manual rain gauge installed to check the accuracy of the tipping bucket rain gauges. ISCO samplers were also installed in the basins (except Borrow Pit) to collect water samples during storm events at the entrance and exit (skimmer) to the basins for another project.

A DJI Phantom 4 RTK UAV (drone) was used to capture images of the drainage area into each basin. This data was processed with image stitching software (Agisoft Metashape), and then imported into Arc GIS software. Digital elevation models, water flow path models, and drainage area was determined using this software for each basin.

Basin water level data, rainfall data, and drainage area was used to calculate the amount of runoff captured by the basins for selected storm events. The total volume of rainfall into the basin watershed was also calculated. For each 5 minute date interval, the amount of rain that fell was converted to feet and then multiplied by the area of the basin watershed area to get the total volume of rain falling into the drainage area in cubic feet. These 5 minute volume intervals were accumulated to get volume of rainfall per time. Only events that did not overtop the auxiliary spillway were included, since we were not monitoring flow from the basin but only water levels.

The basin water level data was used to calculate the volume of runoff entering the basin. For each 5 minute interval, the difference in water level (ft) was multiplied by the average of the water surface area for the two water levels. These volumes were then corrected by adding the volume of water exiting through the skimmer (at greater than 1.5' depth) and subtracting the volume of rain that fell into the basin. Skimmer volume flow was estimated by analyzing the drawdown rate of the basin similar to the inflow rate just described. The dimensions of the basin water surface were measured at a given depth of water in the field. Based on the slope of the basin sides (2:1), a linear regression was created to calculate the area of the water surface in the basin for any level (Table 3.0, Figure 3.0). The runoff volume for each 5 minute interval was accumulated to get runoff volume with time. This data was plotted with the rainfall volume with time. The difference between these two lines can then be used to estimate the percentage of runoff.

Table 3.0. Example of area calculations for the basins based on depth and resulting area.

Basin Depth	Width	Length	Area
	ft		ft ²

1	30	60	1800
1.5	32	62	1984
2	34	64	2176
2.5	36	66	2376
3	38	68	2584

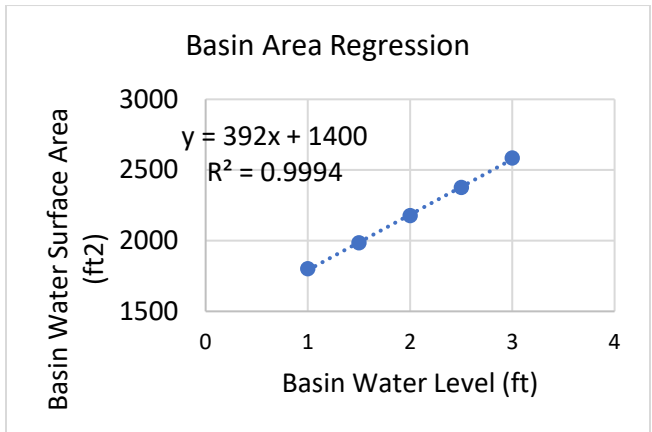


Figure 3.0. Regression of basin water level with volume in the basin.

Two pairs of basins were monitored on the I-540 project near Garner (Figs. 3.1-3.4) and a borrow pit basin (Fig. 3.5) was monitored on the US 401 widening project. All basins had the skimmer outlet set at one foot, so depth changes are from that point since there was a standing pool between events.



Figure 3.1. Picture of Basin 1 after a runoff event. Heavy winds were creating a choppy surface.



Figure 3.2. Picture of Basin 2 between runoff events.



Figure 3.3. Picture of Basin 3 at one of the two inlets. Sampler tubing can be seen along the top of the first baffle.



Figure 3.4. Picture of Basin 4 showing the samplers and rain gauges.



Figure 3.5. Picture of Borrow Pit Basin during skimmer discharge period.

Results

The watershed areas estimated from the UAV surveys ranged from 2.4 to 9.9 acres (Table 3.1). The Borrow Pit basin had active grading and excavating in its watershed which resulted in highly variable drainage areas. During the period of monitoring, Basins 1-4 had relatively little grading and changes to their watersheds and much of the area was stabilized with vegetation or ground wood mulch. An example of the watershed delineation results is shown in Figure 3.6 for Basin 2.

Table 3.1. Watershed areas for the monitored basins based on GIS modeling.

	Approximate Basin Dimensions (ft)	Watershed Area (acres)	Volume at Auxiliary Spillway Weir (ft ³)
Basin 1	65 x 100	2.4	6350
Basin 2	63 x 125	8.8	24765
Basin 3	50 x 100	5.7	14976
Basin 4	50 x 100	6.0	15435
Borrow Pit	75 x 110	.25 to 9.9	19157

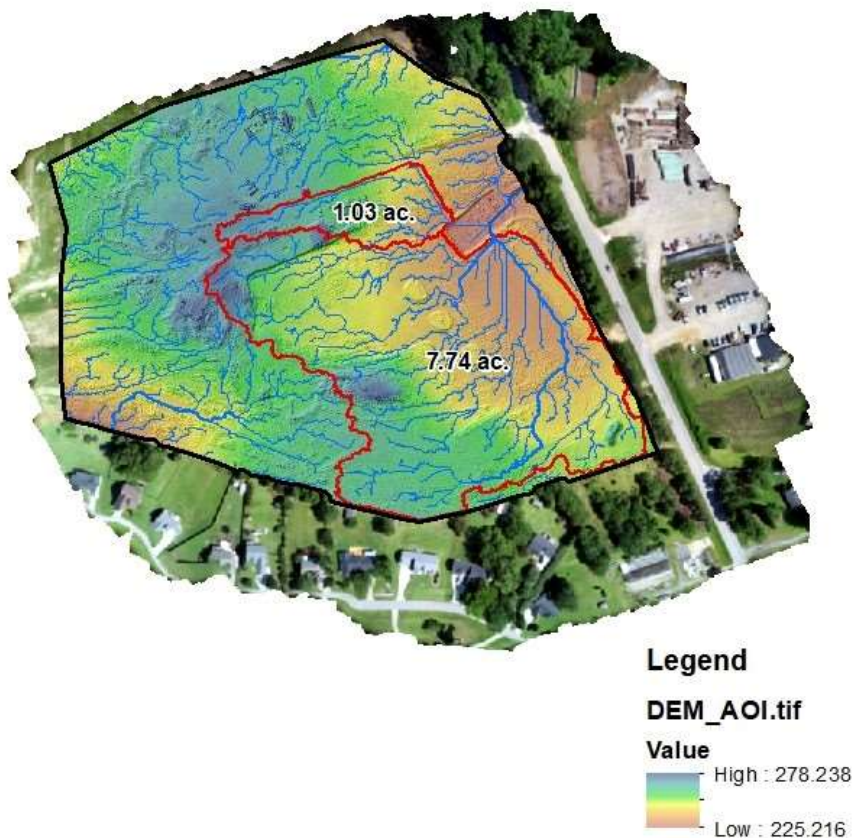


Figure 3.6. Watershed for Basin 2, showing the two different drainage areas.

The water levels in Basins 1 and 2 closely followed the rainfall patterns, as expected (Fig. 3.7). The two basins responded similarly to rainfall in the rising limb of water level but Basin 1 drained more slowly than Basin 2. The effect of rainfall patterns and different environmental conditions was evident. An April event produced a little over an inch of rain over about 12 hours, with peak rainfall intensity of 0.4 in hr^{-1} (Fig. 3.8) while a similar amount fell mostly in a 20 minute period in July (Fig. 3.9). It took about three hours for Basin 1 to begin to rise in April but only 20 minutes in July. Much more of the runoff made it to the basin in April (44%) compared to July (25%), possibly due to drier soil or other changes in the site. The patterns for these two storms were quite similar in Basin 2, adjacent to Basin 1, except that only about half as much of the rain volume made it into the basins (Figs. 3.10-3.11).

The Borrow Pit Basin was monitored for about six months from March – September 2020, with 10 events resulting in flow to the basin (Fig. 3.12). Relatively little of the rainfall volume made it into the basin, with about 20% reaching the basin in three storms at different times (Figs. 3.13-3.15). All three of these storms had rainfall spread over relatively long spans of time, which may have been responsible for the low runoff amounts due to infiltration, evaporation, and storage.

Basin 3 and 4 were monitored for approximately nine months from July 2020 to March 2021, during which there were nearly 20 events that resulted in a rise of more than one foot (Fig. 3.16). The watersheds of these basins were long and narrow compared to the others, and disturbance was mostly from an access road for construction of a culvert and a small borrow area. The amount of rainfall that flowed into the basins is shown for two different types of events, a gentle rain of 0.76" (Figs. 3.17 and 3.19) and a storm with higher intensities and rainfall totals (Figs. 3.18 and 3.20). The increased volume in the basins represented 35-50% of the rainfall volume for these two storms, with basin water levels reflecting the rain intensities.

An example of basin water levels during an overtopping event is shown in Figure 3.21 for a 6 inch storm which occurred over a little more than 24 hours. Six hours into the storm the basin began to discharge over the dam weir, then water levels began to drop when the rain was less intense in more intermittent. Once a second round of intense rain began again, discharge through the weir began again. During the second round of intense rainfall, the basin appears to have a negative runoff rate (net discharge) but this is because of slight fluctuations in water levels during weir discharge. Again, we were not measuring flow but just water levels so runoff cannot be estimated while discharges occur through the weir.

Conclusions

The basins studied responded to rain events as expected, with runoff from low-intensity storms ($<1'' \text{ hr}^{-1}$) reaching the basins hours after rain began, but much more quickly during higher intensity storms. For the storms evaluated, which included only those that did not overtop the auxiliary weir, only 50% or less of the rain volume reached the basins. The remaining volume was stored in the watershed, infiltrated, or evaporated. This suggested that curve numbers for similar construction sites may be lower than many have assumed.

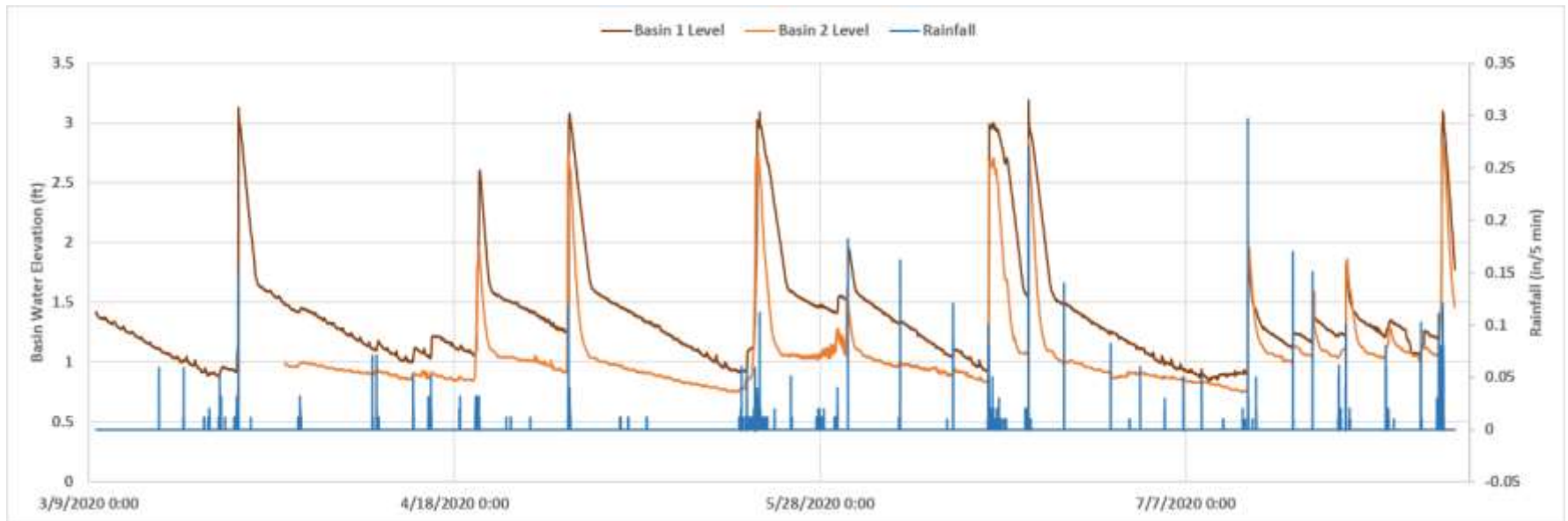


Figure 3.7. Basin water level and rainfall data for Basins 1 and 2 during the monitoring period.

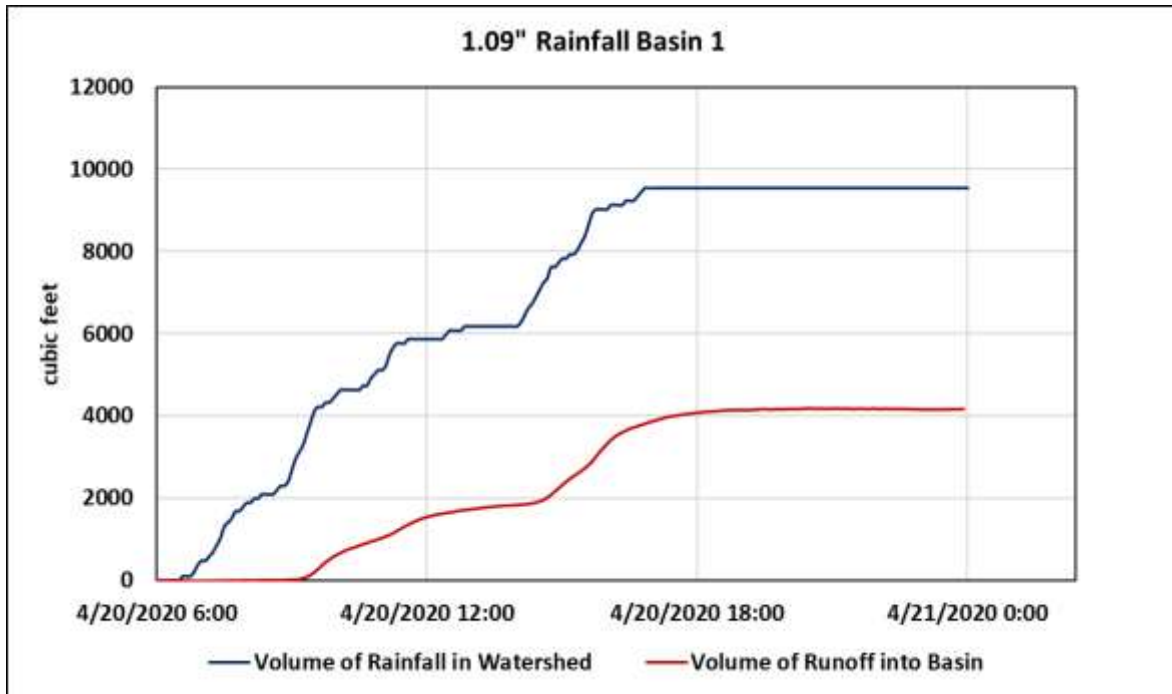


Figure 3.8. Volume of rainfall in Basin 1 watershed and increase in basin volume for the April 20, 2020 storm. Basin volume increase was approximately 44% of rainfall volume.

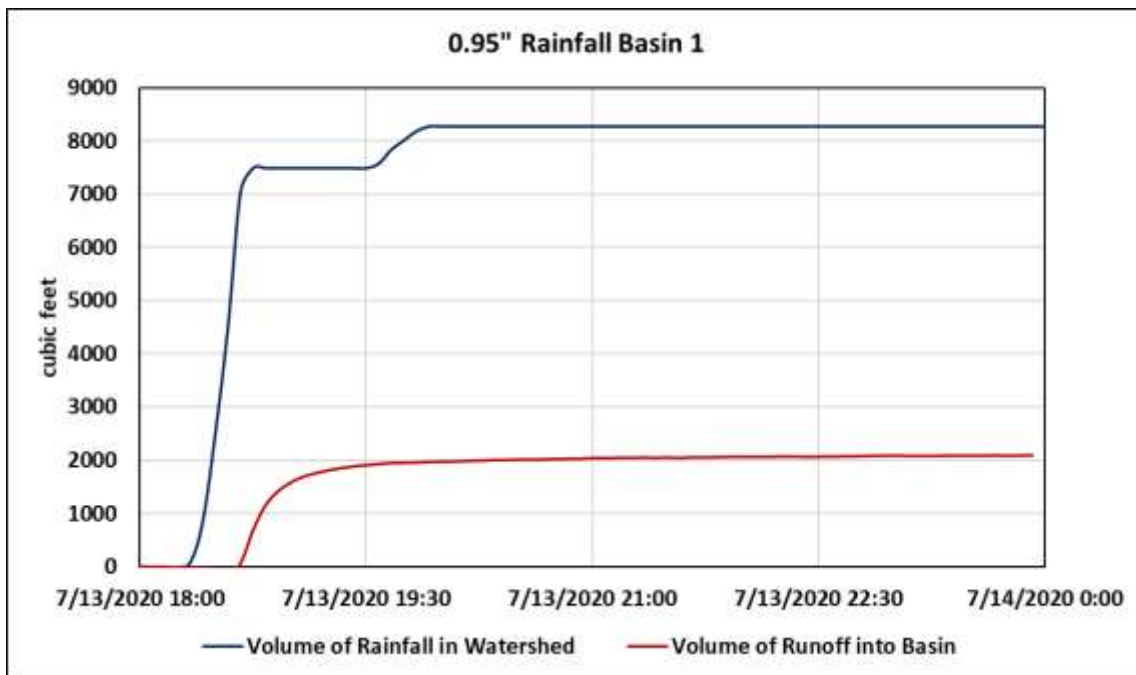


Figure 3.9. Volume of rainfall in Basin 1 watershed and increase in basin volume for the July 13, 2020 storm. Basin volume increase was approximately 25% of rainfall volume.

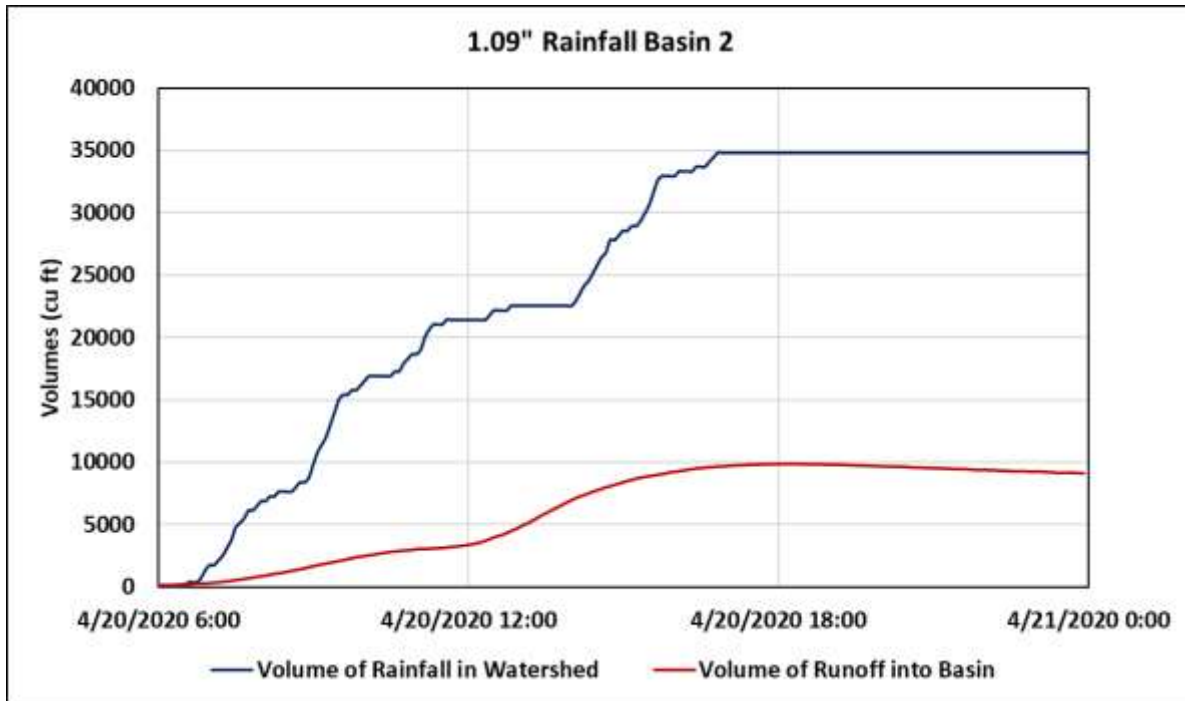


Figure 3.10. Volume of rainfall in Basin 2 watershed and increase in basin volume for the April 20, 2020 storm. Basin volume increase was approximately 26% of rainfall volume.

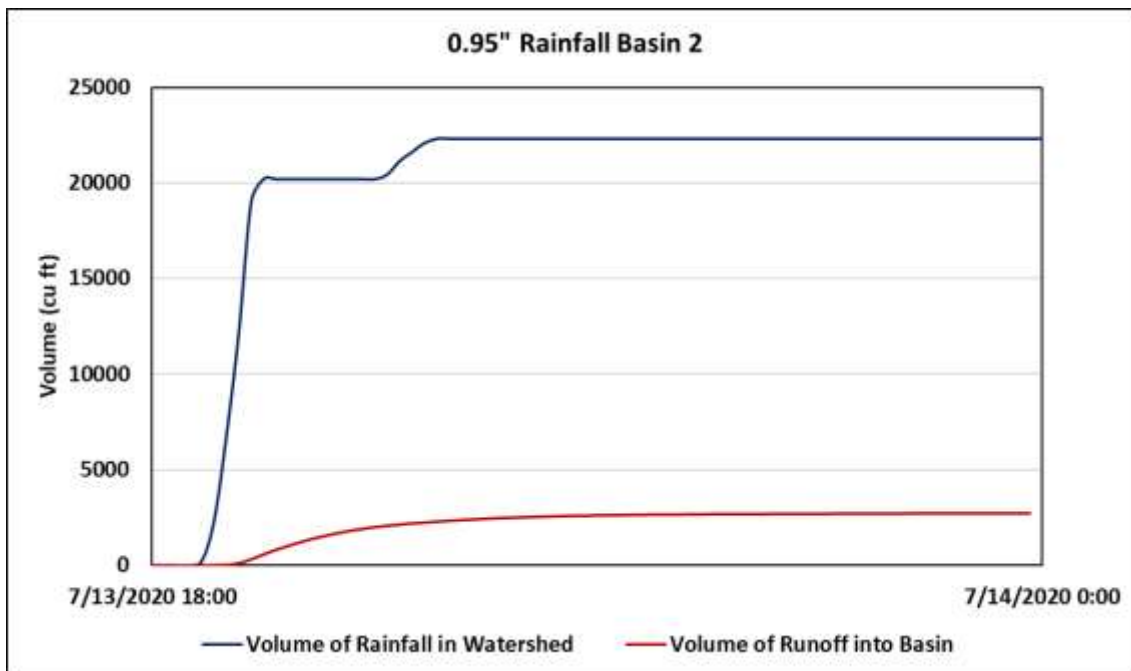


Figure 3.11. Volume of rainfall in Basin 2 watershed and increase in basin volume for the July 13-14, 2020 storm. Basin volume increase was approximately 12% of rainfall volume.

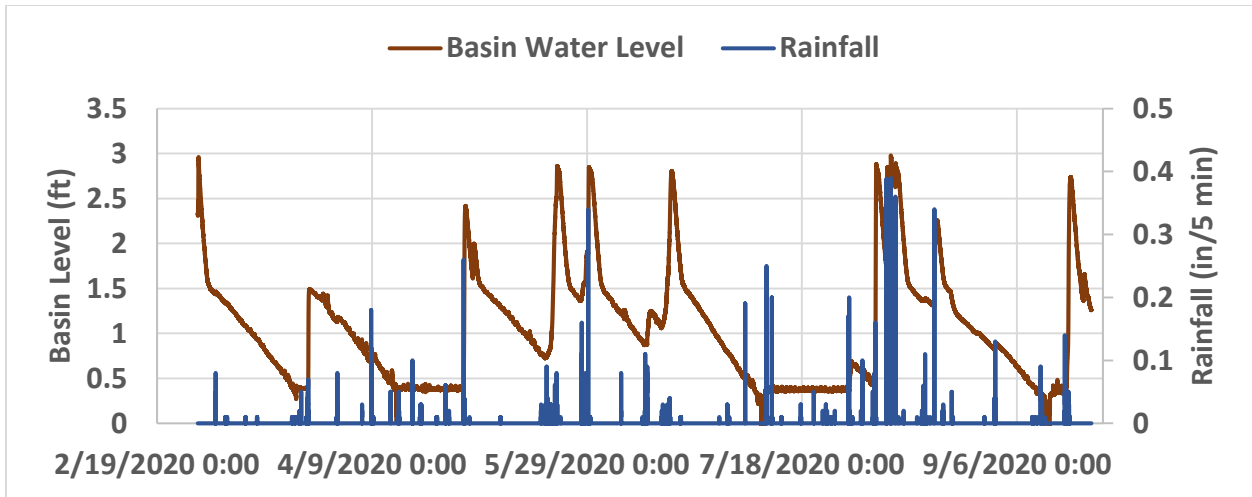


Figure 3.12. Basin water level and rainfall during the monitoring period at the borrow pit on US 401.

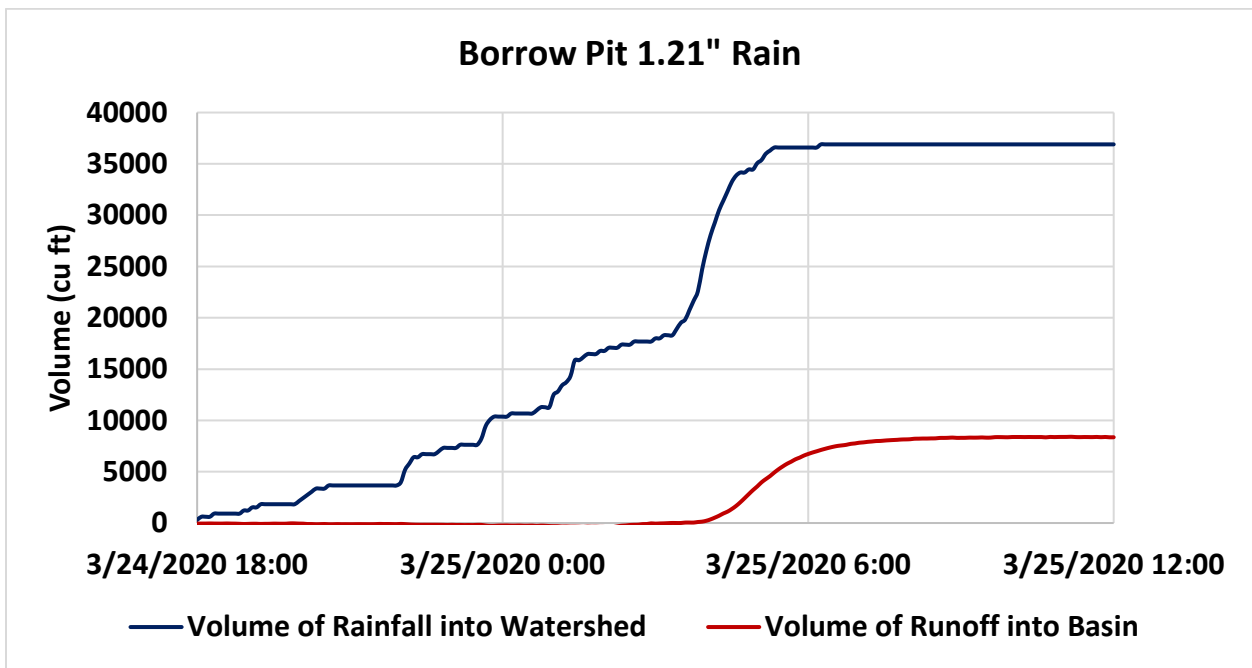


Figure 3.13. Volume of rainfall in the Borrow Pit basin and increase in basin volume for the March 23-25 rainfall event. The drainage area was approximately 8.4 acres for this event. Basin volume increase was approximately 23% of rainfall volume.

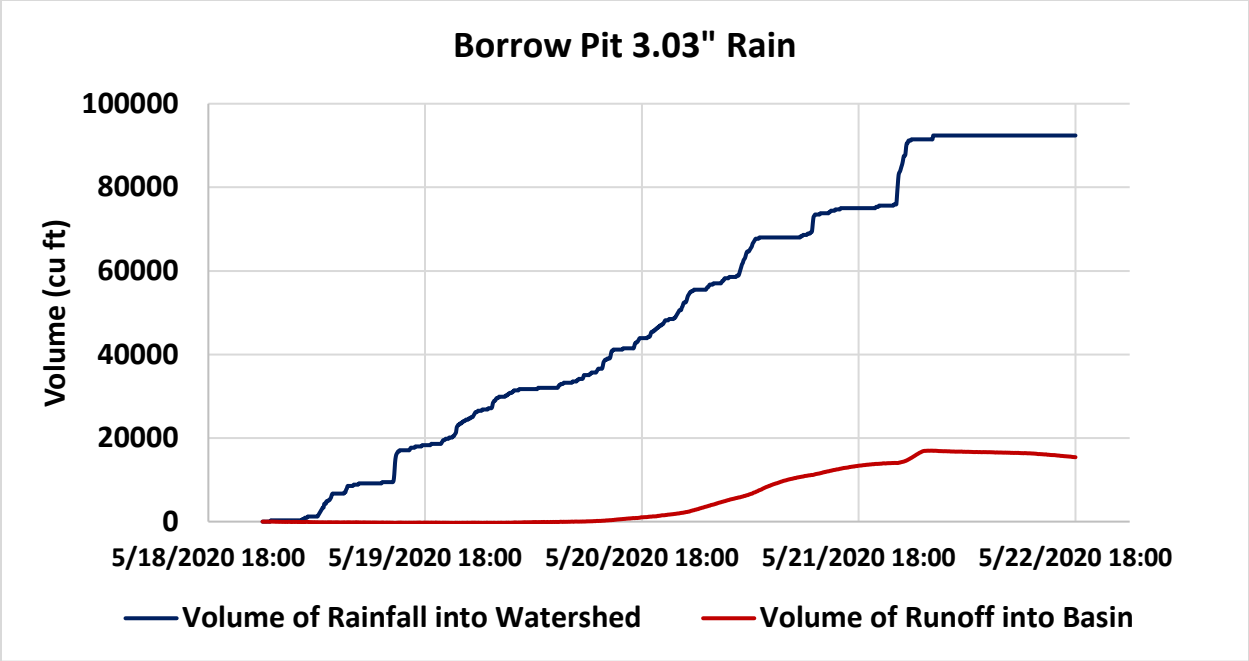


Figure 3.14. Volume of rainfall in the Borrow Pit basin and increase in basin volume for the May 18-21 rainfall event. The drainage area was approximately 9.9 acres for this event. Basin volume increase was approximately 17% of rainfall volume.

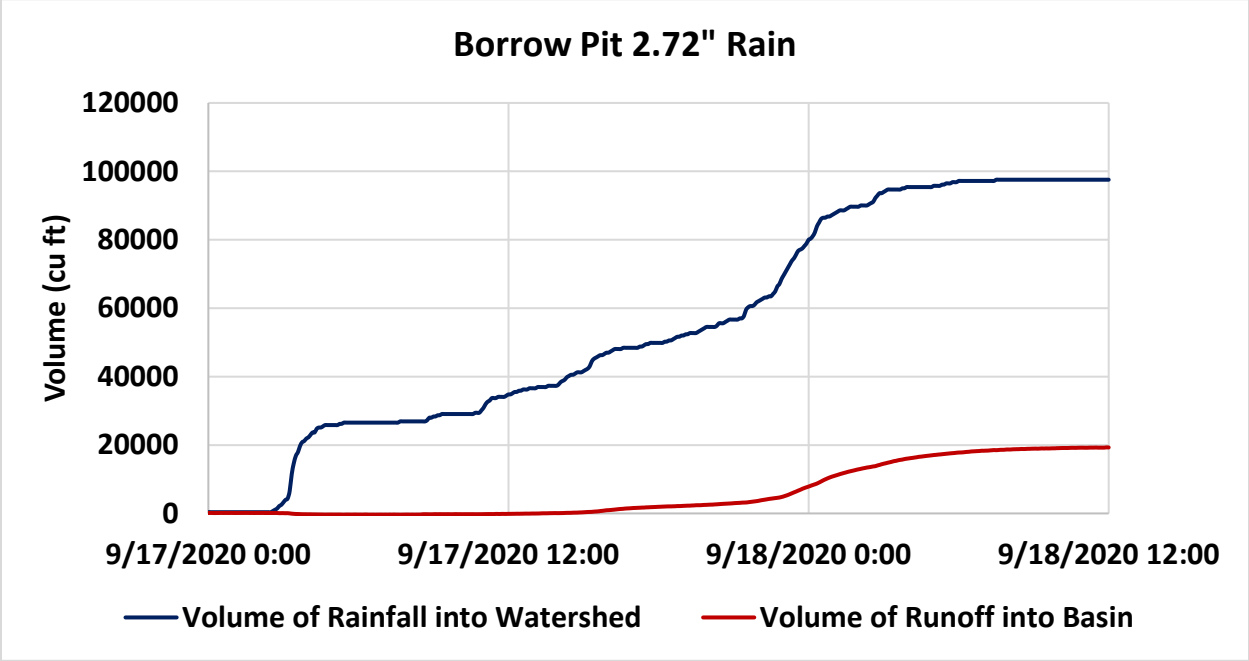


Figure 3.15. Volume of rainfall in the Borrow Pit basin and increase in basin volume for the September 17-18 rainfall event. Basin volume increase was approximately 20% of rainfall volume.

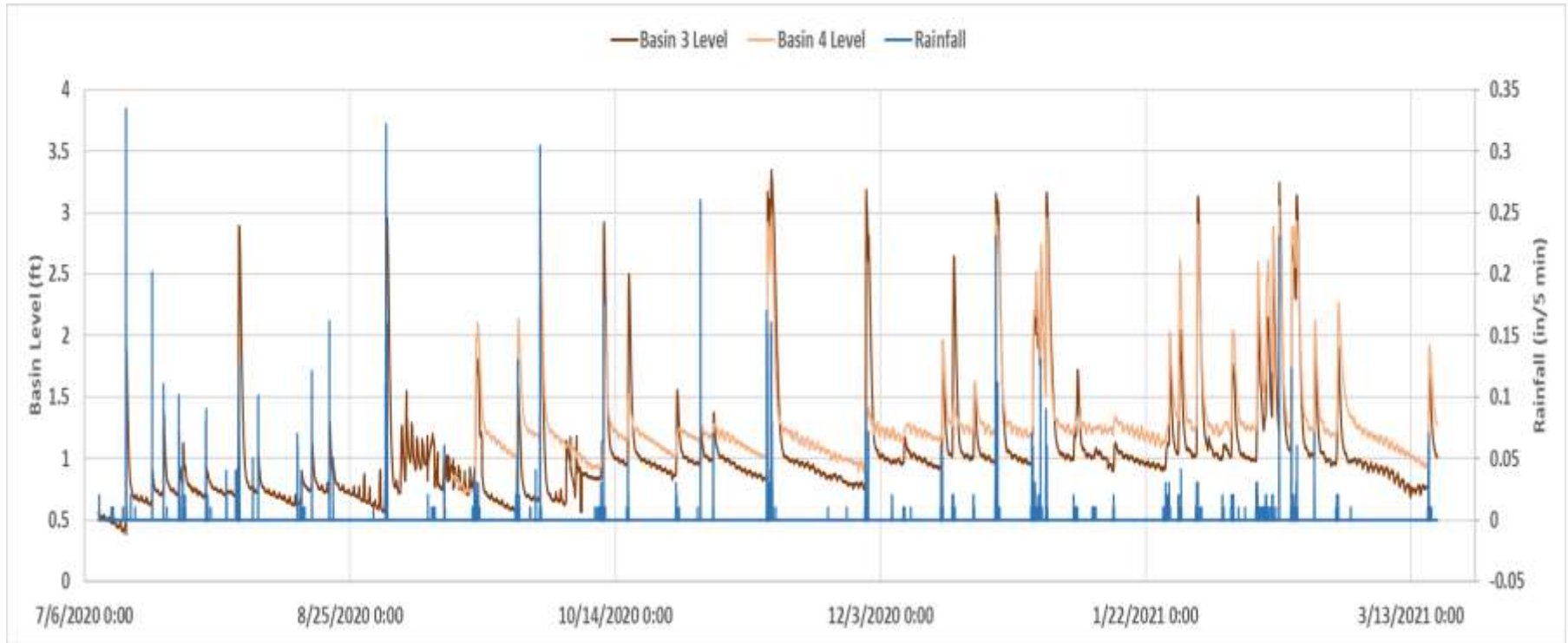


Figure 3.16. Rainfall and basin water levels for the monitoring period of Basins 3 and 4.

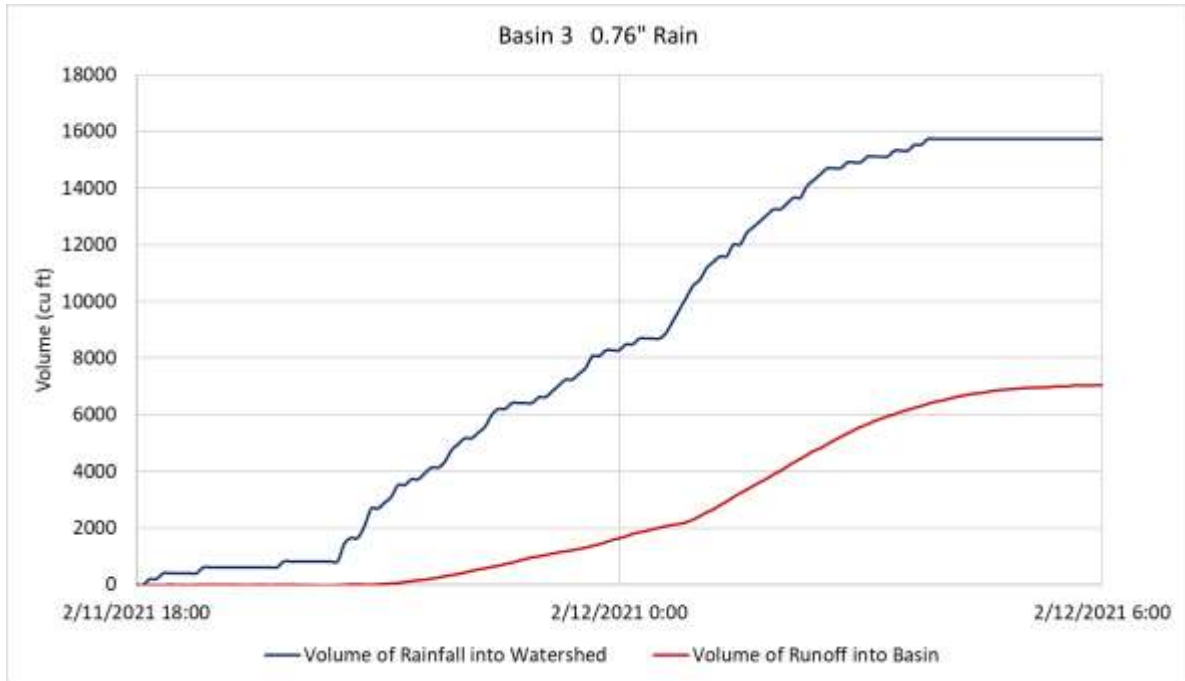


Figure 3.17. Volume of rainfall in Basin 3 and increase in basin volume for the February 12, 2020 rainfall event. Basin volume increase was approximately 45% of rainfall volume.



Figure 3.18. Volume of rainfall in Basin 3 and increase in basin volume for the February 18-20, 2020 rainfall event. Basin volume increase was approximately 37% of rainfall volume.

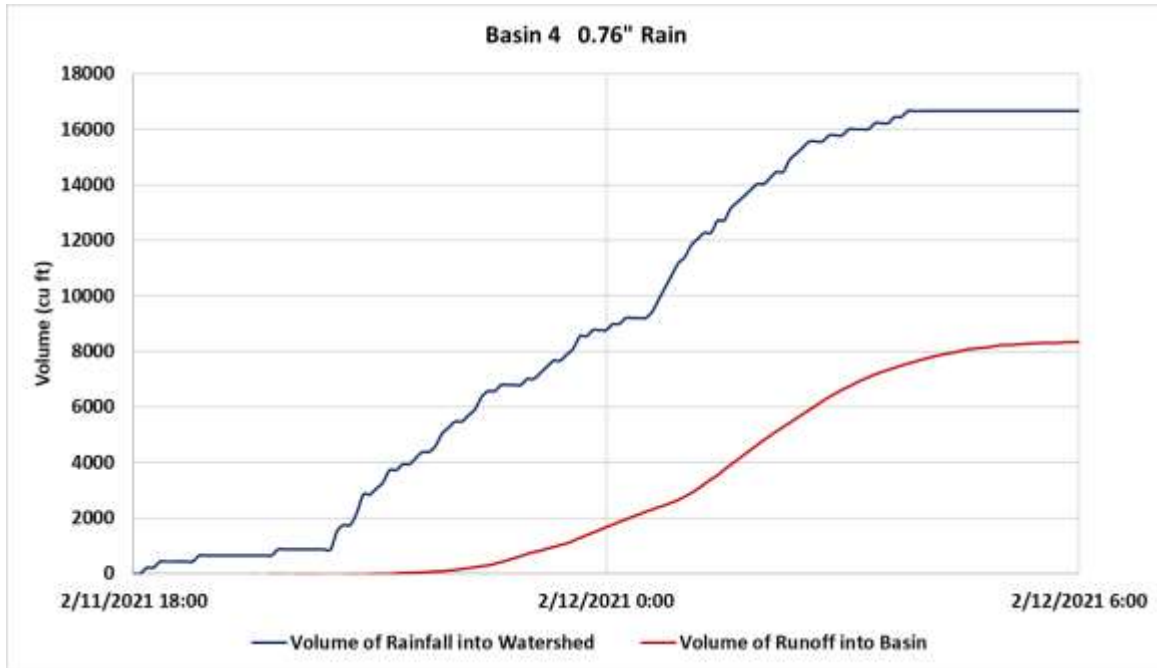


Figure 3.19. Volume of rainfall in Basin 4 and increase in basin volume for the February 11-12, 2020 rainfall event. Basin volume increase was approximately 50% of rainfall volume.



Figure 3.20. Volume of rainfall in Basin 4 and increase in basin volume for the February 18-20, 2020 rainfall event. Basin volume increase was approximately 34% of rainfall volume.

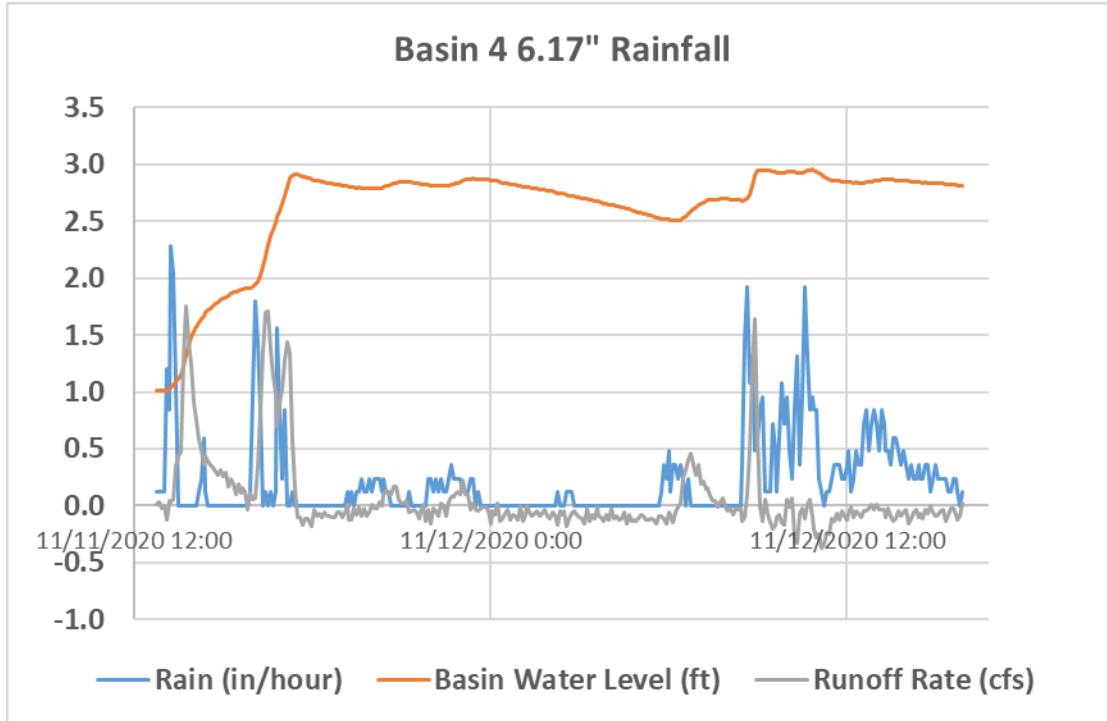


Figure 3.21. Rainfall rate, basin water level, and estimated runoff rate for Basin 4 during a 2-day rain event totaling 6.17 inches of rain. Discharge over the weir occurred slightly lower than three feet.

Chapter 4: Fence Post Testing

This chapter was prepared by:

Gregory Lucier, Ph.D., Laboratory Manager

Johnathan McEntire, Laboratory Technician

Austin Luong, Student Laboratory Assistant

Department of Civil, Construction, and Environmental Engineering

Introduction

A traditional silt fence must resist lateral loads created by the hydrostatic pressure of impounded liquid (a mixture of water, silt, and other debris). The retained liquid acts against the reinforced fabric which in turn transfers loads to the silt fence posts. These posts must then carry the loads into a foundation, almost always the post itself driven into unreinforced earth. Of interest to the current study is the structural performance of the posts and, more specifically, whether renewable wooden posts can deliver appropriate strength for use in NCDOT silt fences. As such, the current study focuses on post strength and does not consider the interaction of posts with the supporting soil. Soil type, soil moisture, and post base configuration will be the major factors in determining whether available soils on a given site can support a selected post. For example, a post with a plate at the base will engage better with loose and/or moist soils than will the same post without a plate. Similarly, a selected post may be able to achieve adequate support without a plate in relatively firm and/or dry soil. The geometry of the post itself will also factor in to the interaction with the supporting soil. In general, posts with thin sections and sharp edges will engage less well with the surrounding soil than will posts with broad and flat cross sections. A detailed study of the interaction between posts and soil is outside the scope of the current work.

Relevant Literature

Literature on the structural testing of silt fence posts is limited. Recent work by Whitman et. al. examined various types of posts and collected laboratory data to provide insight on the limit state for each type. From the lab results, these researchers created an equation to calculate post spacing. This prior work considered the post unit weight (pound per foot) as the primary structural property. The current research presented here discusses post strength in terms of fundamental structural properties such as geometric cross-section, material strength, and moment demand as derived from hydrostatic pressure distribution.

ASTM D6461-18 *Standard Specification for Silt Fence Materials*, recommends a minimum 3 ft. length of post for steel, wood, or synthetic posts, but notes that a 4 ft. T-shaped post is most common. North Carolina Department of Transportation (NCDOT) requires a longer length, at least 5 feet, as the post must be driven into the ground at least 2 feet. The EPA (Apr 2012) notes

that driven depth is important for the post to provide sufficient strength to resist tipping from the hydraulic pressure. NCDOT allows for steel posts of a minimum weight of at least 1.25 lbs./ft. and also specifies that posts should have anchor plates (base plates) with an area of at least 14.0 square inches to better engage the post with the supporting soil. NCDOT does not currently allow for the use of wooden silt fence posts. ASTM D6461-18 allows for steel posts “of U, T, L, or C shape” weighing 1.15 lbs./ft. or greater.

When it comes to wooden silt fence posts, ASTM D6461-18 notes that hardwood posts of minimum 1.2” x 1.2” square cross-section or No. 2 Southern Pine posts of minimum 2.5” x 2.5” square cross-section have performed well. The Michigan Department of Transportation (MDOT) standard for silt fences allows for hardwood posts having a minimum square cross-section of 1.125” x 1.125”, less than the ASTM minimum.

Georgia DOT (GADOT) Specifications allow for the use of wooden posts in silt fencing. GADOT Specification *Section 862 – Wooden Posts* is referenced by the silt fencing specification (*Section 171 – Silt Fences*) and notes that Southern Pine should be used for all posts and bracing. However, *Section 862* goes on to list requirements appropriate only for relatively large posts (all posts have metal caps, etc.). *Section 894 – Fencing* is also referenced by *Section 171 – Silt Fences* and contains information specific to silt fence posts (*Section 894.2.06.2*). The *Section 894* requirements vary according to three different fence types – Type A, B, and C. Wooden posts are allowed in Type A and B fences. Steel posts only are allowed for Type C fences. *Section 894* indicates that “post sizes and types as determined by the type of fence being installed. Generally hardwood posts will be limited to ash, hickory, or oak. Other hardwoods may be acceptable if approved by the Office of Materials and Research.”

Relevant portions of the GADOT post requirements then explicitly allow softwood posts as summarized in Table 4..

Table 4.0: GADOT Silt Fence Post Requirements (Specification Section 894)

<u>GADOT Silt Fence Type</u>	<u>Allowable Materials and Length</u>	<u>Allowable Cross-Sections</u>
Type A	Wood or steel, at least 4 ft. long	Softwood posts at least 3” in diameter or nominal 2” x 4” and straight enough to provide a fence without noticeable misalignment. Hardwood posts that are 1.5” x 1.5” with a minus tolerance of 0.25” providing the cross sectional area is at least 2.25 in ² (1440 mm ²).

		Steel posts with “U,” “T,” or “C” shaped cross-section with a minimum weight of 1.15 lb/ft.
Type B	Wood or steel, at least 3 ft. long	Softwood posts at least 2” in diameter or nominal 2” x 2” square. Hardwood posts at least 1” x 1” square with a minus tolerance of 0.25” providing a minimum cross sectional area of 1 in ² . Steel posts with “U,” “T,” or “C” shaped cross-section with a minimum weight of 0.75 lb/ft.
Type C	Only steel, at least 5 ft. long	Use “U,” “T,” or “C” shaped posts w/ minimum weight of 1.15 lbs. per foot.

Thus, current NCDOT Specifications for post weight and dimension appear to be more conservative than both the ASTM Standard and other DOT specifications including Michigan and Georgia.

Loads Acting on a Silt Fence Post

To evaluate silt fence post strength, one must first define the applied loads that a silt fence post must support. It is also useful to express those loads in terms of applied moment and applied shear on a single post. The applied load on a single silt fence post will generally be a function of the height of liquid retained by the fence and the spacing between adjacent fence posts. As with all hydrostatic pressure problems, the force on a given post is not related to the expanse of water retrained in a horizontal plane. Water pressure acting along the height of the post is a function only of the height of retained water, and the pressure variation will take the form of a triangular pressure distribution, as shown in Figure 4.. The total volume of the retained water does not factor in. The lateral pressure acting at a height equal to the water surface will be zero. The lateral pressure acting at the bottom of the bottom of the retained liquid will be equal to the density of the liquid multiplied by the height of the liquid. For a silt fence subjected to the most severe service condition, the water height will equal the fence height. Thus, the peak pressure at the bottom of the distribution is expressed by *Equation 4.* For a standard fence height of 2 ft., the maximum pressure acting at the bottom of the distribution is 124.8 psf (or lbs. per square foot) and the pressure acting at the top of the distribution is 0. Since the distribution is triangular, its centroid is located at a distance of 1/3H from the bottom.

<p>Where:</p> <p>P is the lateral pressure (psf or lbs. per ft.²)</p> <p>ρ is the density of retained liquid, assumed 62.4 (lbs./ft.³) for water</p> <p>H is the fence height in (ft.)</p>	$P = \rho H$ <p>Equation 4.0</p>
--	---

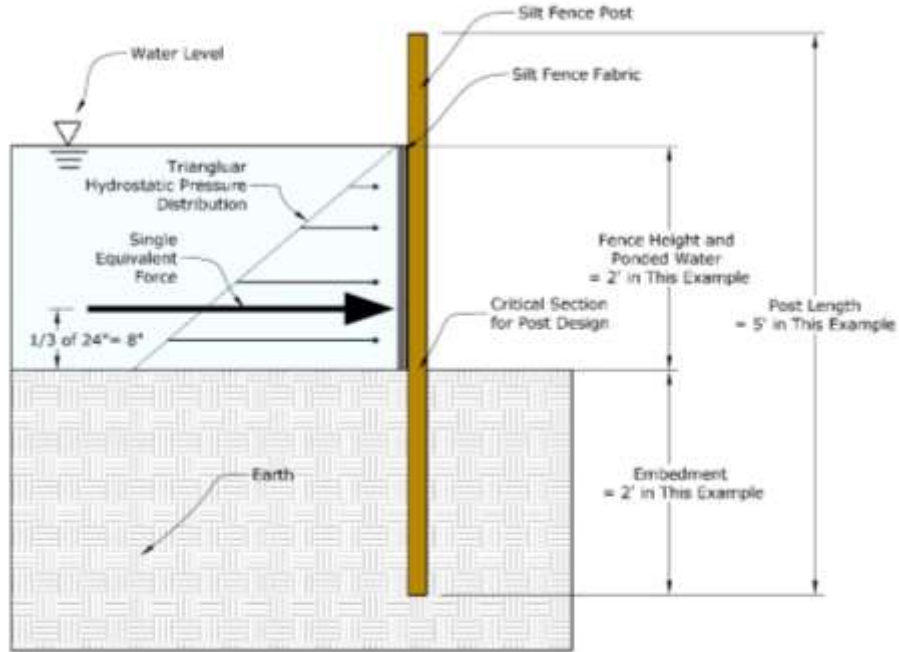


Figure 4.0: Simplified Fence Post Loading Model, Profile View

The pressure distribution described above acts over a tributary area defined by the fence height and post spacing. Each fence post supports an area of fence (and the pressure acting on that area) that is “S” feet wide and “H” feet tall, where “S” is the spacing between posts and “H” is the fence height, as shown in Figure 4.. Note that if the height of the retained water is less than the fence height, then the height of the retained water should be used instead. We will call the height of the retained water “W”.

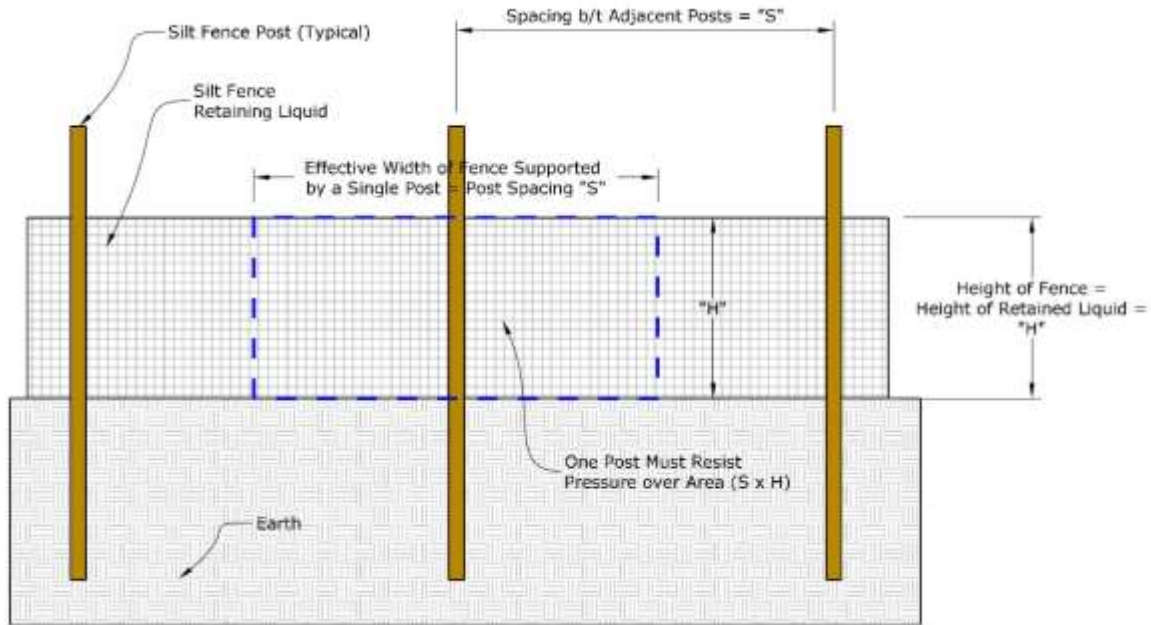


Figure 4.1: Simplified Fence Post Loading Model, Elevation View

Considering Figure 4. and Figure 4., the total load acting on an individual fence post is expressed by *Equation 4.*. If the fence height is assumed as 2 ft., post spacing is assumed to be 8 ft., and the peak pressure is known to be 124.8 psf, then the maximum total load a single post may have to safely support is 998.4 lbs. This load would act at the centroid of the triangular pressure distribution at a location 1/3 of the way up the post from the ground surface (8"). Stated otherwise, if a 2' tall silt fence with 8' post spacing were overtopped with water, that fence would collapse if each post were not able to support a lateral load of at least 999 lbs. Table 4. summarizes the maximum peak equivalent loads acting on a single post for various combinations of post spacing and retained water height.

$F = \frac{1}{2} P(WxS)$	<i>Equation 4.1</i>
<p>Where:</p> <p>F is the equivalent force acting on a given post (lbs.)</p> <p>P is the peak lateral pressure, described by Equation 4. in (psf)</p> <p>W is the height of retained water in (ft.), equal to a maximum of the fence height H in severe cases</p> <p>S is the spacing between adjacent fence posts (ft.)</p>	

Table 4.1: Total Force on a Single Post by Water Height and Post Spacing

Total Equivalent Force “F” on a Single Post (lbs.)		Spacing between Adjacent Posts (ft.)				
		4'	5'	6'	7'	8'
Height of Ponded Water (ft.)	0.25 ft. (= 3")	8 lbs.	10 lbs.	12 lbs.	14 lbs.	16 lbs.
	0.5 ft. (=6")	31 lbs.	39 lbs.	47 lbs.	55 lbs.	62 lbs.
	0.75 ft. (=9")	70 lbs.	88 lbs.	105 lbs.	123 lbs.	140 lbs.
	1 ft.	125 lbs.	156 lbs.	187 lbs.	218 lbs.	250 lbs.
	1.25 ft.	195 lbs.	244 lbs.	293 lbs.	341 lbs.	390 lbs.
	1.5 ft.	281 lbs.	351 lbs.	421 lbs.	491 lbs.	562 lbs.
	1.75 ft.	382 lbs.	478 lbs.	573 lbs.	669 lbs.	764 lbs.
	2 ft.	499 lbs.	624 lbs.	749 lbs.	874 lbs.	998 lbs.

Note: The force is assumed to act at the pressure centroid = 1/3 of the water depth

To size a fence post, the information in Table 4. can be converted to moments and shears acting at the base of the post. Since posts act as cantilevers, the maximum moment and the maximum shear both occur at the bottom of the post. Stated otherwise, the bottom of the post is the most critical section, so a post with a consistent cross-section would break at the bottom if overloaded. Moment is expressed in ft.-lbs. and quantifies the bending demanding on a post. Shear is expressed in lbs. and simply equals the maximum force on the post as expressed by *Equation 4.*. The moment capacity of a cantilever is usually more critical than shear capacity.

<p style="text-align: center;">$M = F(1/3xW)$</p> <p>Where:</p> <p>M is the maximum moment subjected to the post (lbs.-ft.)</p> <p>F is the magnitude of the equivalent force acting on a given post (lbs.)</p> <p>W is the height of retained water in (ft.), equal to a maximum of the fence height H in severe cases</p>	<p>Equation 4.2</p>
--	----------------------------

The constant (1/3) comes from the location of the centroid of the pressure distribution, as shown in Figure 4..	
---	--

Table 4.2: Maximum Moment Demand for a Single Silt Fence Post

Maximum Moment Demand “M” on a Single Post (ft.-lbs.), per Equation 4.		Spacing between Adjacent Posts (ft.)				
		4’	5’	6’	7’	8’
Height of Pounded Water (ft.)	0.25 ft. (= 3”)	0.7	0.8	1.0	1.1	1.3
	0.5 ft. (=6”)	5.2	6.5	7.8	9.1	10.4
	0.75 ft. (=9”)	17.6	21.9	26.3	30.7	35.1
	1 ft.	41.6	52.0	62.4	72.8	83.2
	1.25 ft.	81.3	101.6	121.9	142.2	162.5
	1.5 ft.	140.4	175.5	210.6	245.7	280.8
	1.75 ft.	223.0	278.7	334.4	390.2	445.9
	2 ft.	332.8	416.0	499.2	582.4	665.6

Note: The maximum moment is assumed to act the base of the post

Experimental Program and Specimens

The above analysis forms the basis for the experimental program presented here. In this program, individual silt fence posts were tested to failure to evaluate their peak load and peak moment capacities. All posts were obtained commercially in the Raleigh, NC market. Test specimens were selected in each of five styles, some NCDOT approved and some not. Some wooden posts were tested and some steel posts. Southern Pine posts were not available commercially. Five identical replicates of each style post were tested.

Table 4.3 outlines the tested silt fence posts. Typical examples of each style of tested post are documented in Table 4. and

Table 4.. Posts were photographed, average weight per foot measured, and average cross-section dimensions measured.

Table 4.3: Styles of Silt Fence Post Tested

<u>Arbitrary Specimen Group ID</u>	<u>Material</u>	<u>Cross-Section</u>	<u>DOT Approval</u>	<u>Overall Length</u>	<u>Description</u>
S1	Steel	T-shaped, no plate	None	5 ft.	Unpainted Green Resource #000500
S2	Steel	T-shaped with anchor plate	NCDOT	5 ft.	Painted green with white top, 1.25 lbs./ft. nominal Green Resource #000499
S3	Steel	T-shaped with anchor plate	None	5 ft.	Painted green with yellow top, 1.25 lbs./ft. nominal Agri-Supply #10781
W1	Hardwood, species unknown	Square	GA DOT	3 ft.	Agri-Supply #40615, Sold with silt fence fabric
W2	Hardwood, species unknown	Square	None	3 ft.	Agri-Supply #32382, Sold with silt fence fabric

Table 4.4: Photographs of Typical Tested Silt Fence Posts

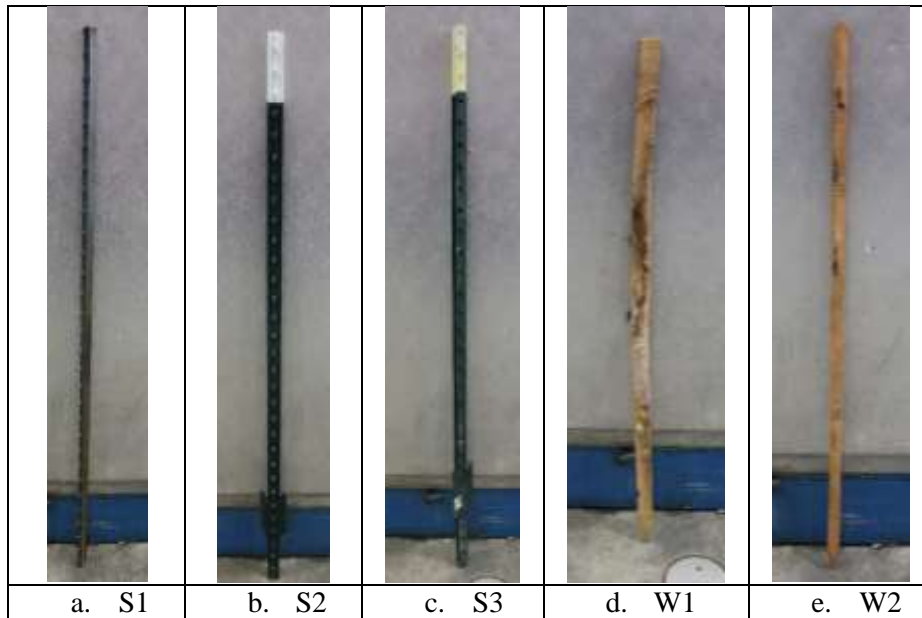


Table 4.5: Properties of Tested Silt Fence Posts

<u>Arbitrary Specimen ID</u>	<u>Cross-Section Sketch</u>	<u>Nominal Weight per Foot</u>	<u>Measured Weight per Foot</u>	<u>Nominal Dimensions</u>	<u>Cross-Section Photo</u>
S1	T-shaped	Not listed	0.87	1.12" tall x 1.22" wide	
S2	T-shaped with plate at bottom	1.25 #/ft.	1.26	1.12" tall x 1.54" wide	
S3	T-shaped with plate at bottom	1.25 #/ft.	1.41	1.26" tall x 1.36" wide	
W1	Square	Not listed	0.67	1.5" x 1.5"	
W2	Square	Not listed	0.24	1" x 1"	

Per the analysis presented above, an experimental test setup was designed to apply a single equivalent applied lateral load on a single silt fence post to failure. This experimental load was configured at a distance 8” above the fixed base of the post to create an applied moment to shear ratio on each post that exactly matches the real distributed loading condition. In simple terms, this means that the experimentally obtained loads can be compared directly to the demand loads outlined in Table 4.. Due to the loading configuration, deflections measured in this laboratory setup would not exactly match deflections under equivalent triangular loading.

In all, 25 silt fence posts were loaded to failure using the test setup shown in Figure 4.. The test setup was designed to utilize as reaction points the strong-floor and strong-wall in the structural engineering laboratory. A steel fixture was fabricated and rigidly attached to the laboratory floor. The upper portion of this fixture consisted of a thick-walled steel pipe arranged such that cylindrical concrete post foundations could be slipped snugly into and out of the pipe. Posts were fabricated with cylindrical concrete foundations that were installed one at a time into the steel support fixture so that they cantilevered out of the foundation in a way similar to their in service operating condition. A synthetic loading sling was slipped over the top of the post and was located at a position 8” above the point of fixity. The point of fixity was considered to be the top surface of the concrete foundation – similar to the point where the fence post normally exits well compacted earth.

The opposite end of the synthetic loading sling was attached to a hydraulic cylinder with an integrated electronic loadcell. The hydraulic cylinder was plumbed to a precision hydraulic pump that allowed for slow and consistent loading of the cylinder and sling in tension. As tension was applied to the loading sling, a lateral force was applied to the silt fence post, similar to the loads created in reality by water ponding against a silt fence. An electronic displacement sensor was attached with fishing line to the upper portion of the fence post. The lateral post displacement was measured at this location, 2’ above the fixed post base. A data acquisition system was connected to the loadcell and to the displacement sensor to measure and record the applied lateral load and lateral post deflection in real time. Each post was pulled steadily to failure at a slow rate.

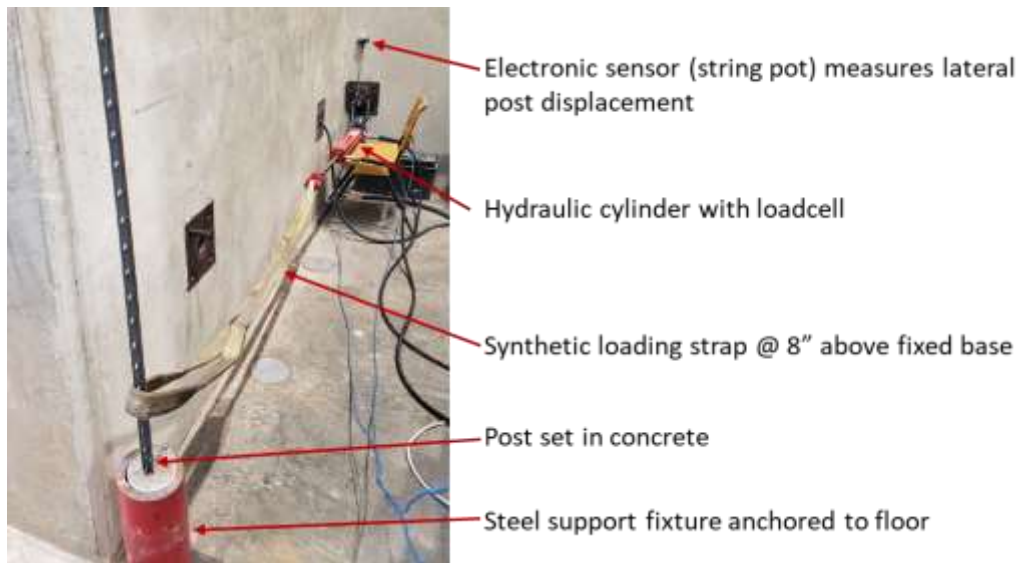


Figure 4.2: Test setup for fence post loading

Test Results

Results from each silt fence post test are summarized in Table 4.. Photographs of the typical failure mode for each type of post are provided in

Table 4.. Load vs. deflection plots for each group of five fence posts are provided in

Table 4..

Table 4.6: Results from Each Silt Fence Post Test

<u>Post Style</u>	<u>Specimen Name</u>	<u>Peak Load (lbs.)</u>	<u>Average Peak Load (lbs.)</u>	<u>Peak Moment (lbs.-ft.)</u>	<u>Failure Mode</u>
S1: T-shaped Steel Post, Non-NCDOT	S1-1	964	968	643	Fracture at post base.
	S1-2	895		597	
	S1-3	995		663	
	S1-4	1016		677	
	S1-5	968		645	
S2:	S2-1	791	1193	528	Yielding at post base with local buckling of the cross-section.
	S2-2	1257		838	
	S2-3	1166		777	

T-shaped Steel Post, NCDOT	S2-4	1361		907	
	S2-5	1392		928	
S3: T-shaped Steel Post, Non-NCDOT	S3-1	1286	1813	858	Yielding at post base with local buckling of the cross-section.
	S3-2	1939		1293	
	S3-3	2173		1449	
	S3-4	1732		1155	
	S3-5	1936		1291	
W1: Wood Post, GADOT	W1-1	431	565	287	Bending then fracture at post base.
	W1-2	749		499	
	W1-3	596		397	
	W1-4	570		380	
	W1-5	482		321	
W2: Wood Post, non-DOT	W2-1	486	325	324	Fracture at post base.
	W2-2	246		164	
	W2-3	428		285	
	W2-4	254		169	
	W2-5	209		140	

Table 4.7: Typical Failure Modes for Each Type of Tested Silt Fence Post

 <p style="text-align: center;">Style S1 Fracture at Post Base (Note post separated from base)</p>	 <p style="text-align: center;">Style S2 Yielding at post base with local buckling of the cross-section.</p>
 <p style="text-align: center;">Style S3 Yielding at post base with local buckling of the cross-section.</p>	 <p style="text-align: center;">Style W1 Bending and Fracture at Post Base</p>

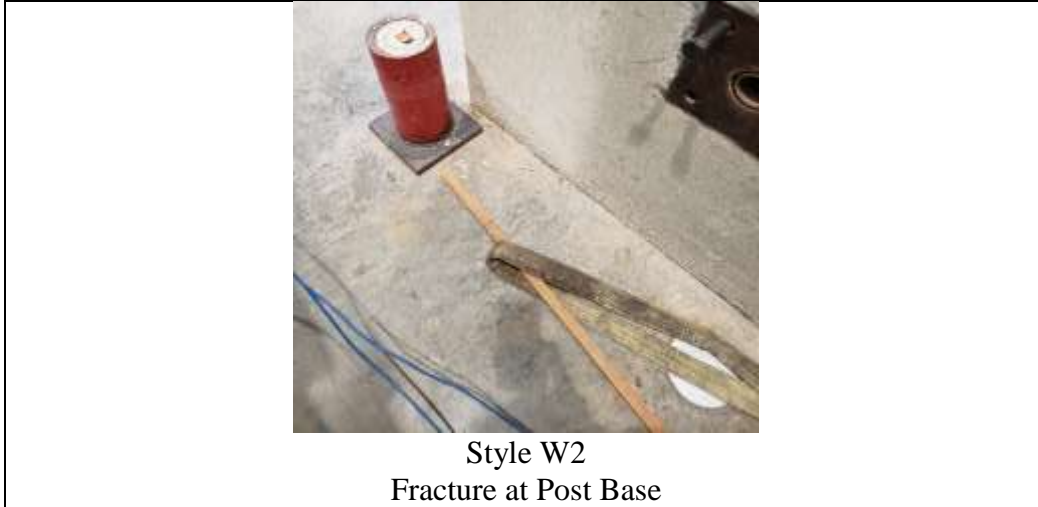
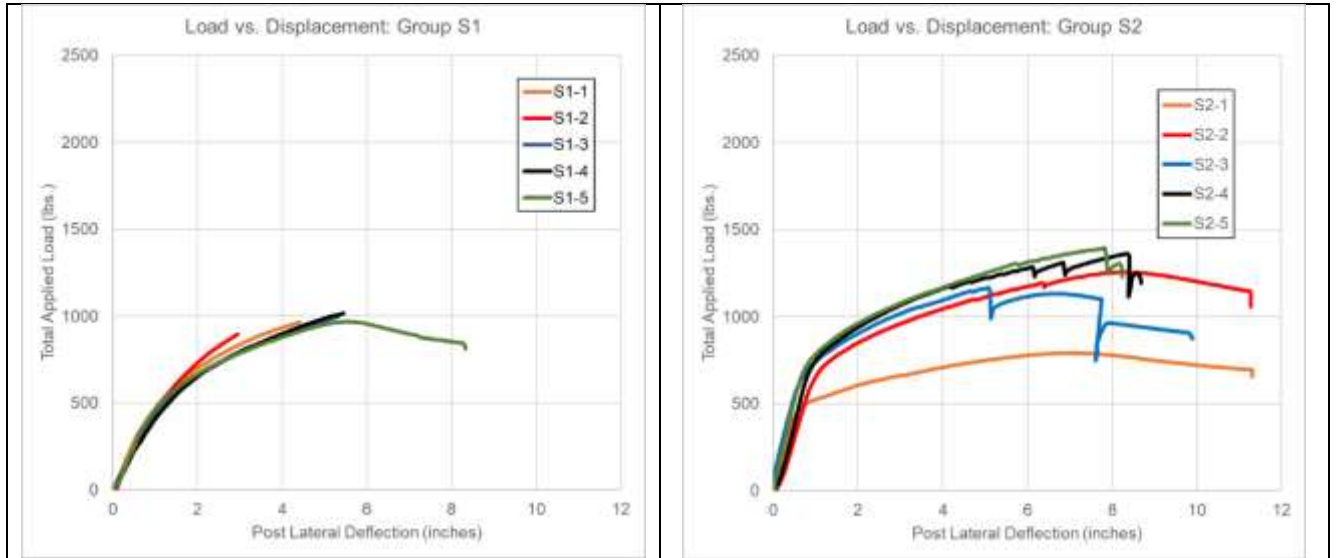
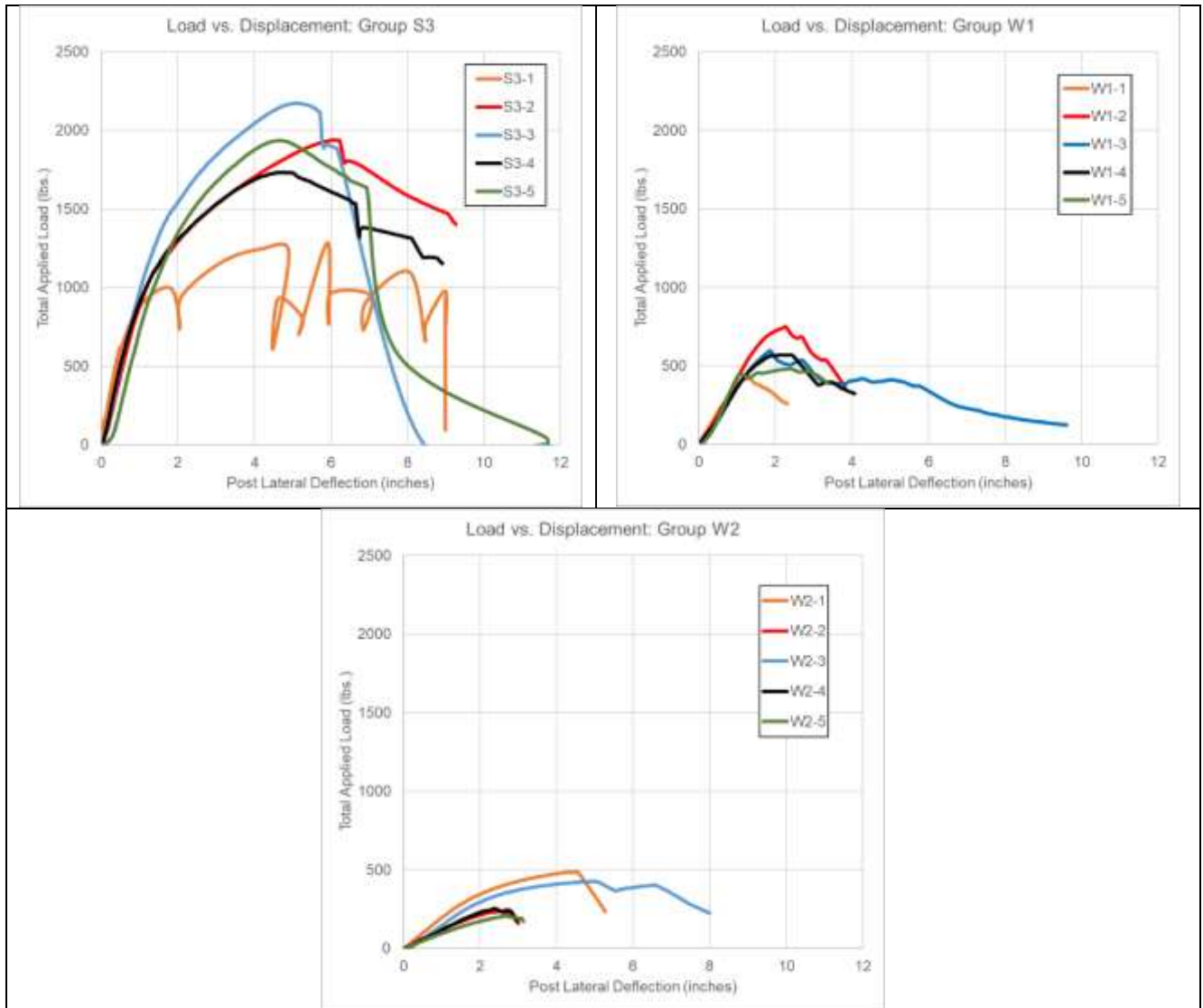


Table 4.8: Load-Deflection Data for All Tested Posts





Analysis and Conclusions

To summarize the test results, all steel posts performed better than both wooden posts in terms of load carrying capacity (see Table 4.). Both steel posts with base plates (NCDOT rated S2 and non-DOT rated S3) achieved peak lateral loads sufficient for supporting 2’ of ponded water at an 8’ post spacing. Of these two posts, the S3 non-NCDOT rated post was significantly stronger than the S2 NCDOT rated post, likely due to higher material strength since both cross-sections had similar dimensions. The failure modes for steel posts involved yielding, fracture, and/or buckling at the post base in the area of maximum applied moment. The load-deflection behavior for all posts shows significant non-linearity prior to failure in all cases, which is a desirable attribute (warning prior to collapse).

Table 4.9: Styles of Silt Fence Post Tested

<u>Arbitrary Specimen Group ID</u>	<u>Material</u>	<u>Cross-Section</u>	<u>DOT Approval</u>	<u>Size or Unit Weight</u>	<u>Average Peak Load (lbs.)</u>	<u>Suitable for 2' of Water and 8' Post Spacing?</u>
S1	Steel	T-shaped, no plate	None	0.87 lbs./ft.	968	No
S2	Steel	T-shaped with anchor plate	NCDOT	1.26 lbs./ft.	1193	Yes (Safety Factor of 1.2)
S3	Steel	T-shaped with anchor plate	None	1.41 lbs./ft.	1813	Yes (Safety Factor of 1.8)
W1	Hardwood, species unknown	Square	GA DOT	0.67 lbs./ft. 1.5" x 1.5"	565	No
W2	Hardwood, species unknown	Square	None	0.24 lbs./ft. 1" x 1"	325	No

Conclusions

The following comments and conclusions are offered in evaluating the experimental results.

- Steel post performance increased with increasing weight per foot. While unit weight per foot is a somewhat unscientific method of specifying steel post performance, it seems to be working in this case, likely because all three metal cross-sections were of similar shapes. A more scientific approach would be to specify the required post moment capacity as a function of post cross-section (moment of inertia) and the yield strength of the post material. However, a more complicated specification would require more complicated QA/QC procedures that may not be warranted.
- Of potential concern is specimen S2-1, an NCDOT rated post. While the average behavior of group S2 achieved the calculated target load, specimen S2-1 failed to reach this target and is a significantly low outlier. A specification for steel posts that measures only post weight per foot creates the possibility for significant variability in performance because variability in key material properties such as metal yield strength will not be

detected. A specification based on cross-section properties and material strengths or on fence post performance (ie: achieve a certain load in a bending test) would more directly test for the primary issue of concern – whether or not each post can hold back the required height of water.

- The average behaviors of the two wooden fence post styles (groups W1 and W2) were at a significantly lower level of performance than that of any steel posts. Likely, neither of these styles of wooden post were intended to retain a full 2' of water.
- The cross-section dimensions required for a Southern Yellow Pine (SYP) post to achieve a lateral load carrying capacity of 999 lbs. in the laboratory test conducted here (required moment capacity of at least 665.6 ft.-lbs.) can be calculated. The section modulus of a square cross-section can be calculated as $b^3/6$ where b is the side of the square. The moment capacity of a square cross-section is defined as $S \cdot F_b$ where S is the section modulus and F_b is the bending capacity (stress) of the material. The maximum bending stress allowed by the *National Design Specification for Wood Construction* for SYP ranges from 850 psi (#3 grade) to 3050 psi (Select Structural). Taking the low end of nominal strength and ignoring some offsetting factors that adjust this nominal value for moisture and short duration loading, we can back-calculate that a SYP post would need to be 3.8" square to safely resist 2' of ponded water. If the high end of the allowable bending stress is assumed, the SYP post would need to be 2.5" square. It is likely that the safety factors included in the bending stress values may be on the high side for silt fences (a non-life safety application), so somewhat smaller post sizes may be acceptable with detailed study. It is, however, unlikely that SYP posts with dimensions substantially smaller than 2" square would be suitable for holding back 2' of ponded water at an 8' post spacing.
- SYP silt fence post cross section sizes could be significantly smaller if less than 2' of ponded water were considered. For example, if only a 1' depth of water needs to be retained, then a Select Structural SYP post of approximately 1.2" square would easily be acceptable using an 8' post spacing. If only 6" of water needs to be retained, then a SYP post only 5/8" square would do the job, still at an 8' spacing. It is noted that a 5/8" square cross-section is likely smaller than what could easily be produced and installed for this application, so a larger cross-section would probably be selected for practical reasons.
- Standards published by ASTM, MDOT, and GADOT allow for the use of wooden silt fence posts, at least in limited situations. In general, there exist appropriate applications for wooden posts when the projected loading demands on a silt fence will be lower than the most severe theoretical values.

Literature Cited

1. ASTM International. D6461/D6461M-18 Standard Specifications for Silt Fence Materials. West Conshohocken, PA; ASTM International, 2018.
2. Michigan Department of Transportation. 2003. Standard Specifications for Construction. Oakland County, Michigan Water Resources Commissioner. Individual Soil Erosion and Sedimentation Details, SP-2-Silt Fence. https://www.michigan.gov/documents/deq/nps-silt-fence_332134_7.pdf
3. Georgia Department of Transportation. Erosion Control Specification Section 171 – Silt Fences (Referencing Section 862 – Wooden Posts and Section 894 – Fencing). Publication date unknown, accessed March 2021. <http://www.dot.ga.gov/PartnerSmart/Business/Source/specs/ss171.pdf>
4. North Carolina Department of Transportation. 2015. *Erosion and Sediment Control Design and Construction Manual*. <https://connect.ncdot.gov/resources/roadside/SoilWaterDocuments/Erosion%20and%20Sediment%20Control%20Design%20and%20Construction%20Manual.pdf>
5. South Carolina Department of Transportation. 2007. Standard Specifications for Highway Construction. Supplemental Technical Specification for Silt Fence Systems, SC-M-815-2. <https://www.scdot.org/business/technicalPDFs/supTechSpecs/SC-M-815-2-silt-fence-spec-0718.pdf>
6. U.S. Environmental Protection Agency 2007. Developing Your Stormwater Pollution Prevention Plan, EPA 833-R-06-004. Washington: EPA. <https://www3.epa.gov/npdes/pubs/siltfences.pdf>
7. Whitman, J. B., W. C. Zech, and W.N. Donald. *Full-Scale Performance Evaluations of Innovative and Manufactured Sediment Barrier Practices*. Transportation Research Record: Journal of the Transportation Research Board, 2019.
8. Whitman, J. B., W. C. Zech, W. N. Donald, and J. J. LaMondia. *Full-Scale Performance Evaluations of Various Wire-Backed Nonwoven Silt Fence Installation Configurations*. Transportation Research Record: Journal of the Transportation Research Board, 2018. 2672(39), 68-78.